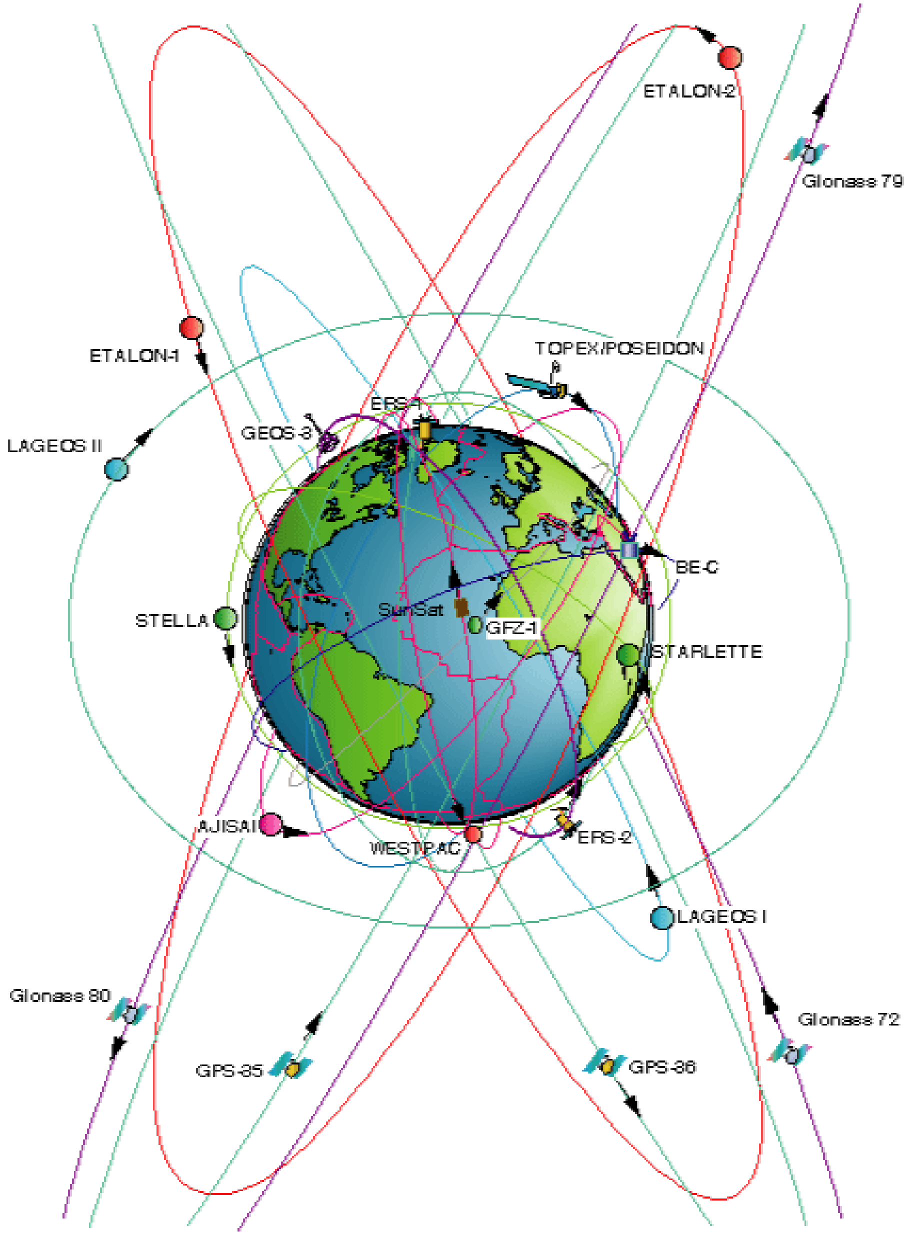

Space Geodesy and Satellite Laser Ranging

Michael Pearlman*
Harvard-Smithsonian Center for Astrophysics
Cambridge, MA USA

*with a very extensive use of charts and inputs provided by many other people

Causes for Crustal Motions and Variations in Earth Orientation

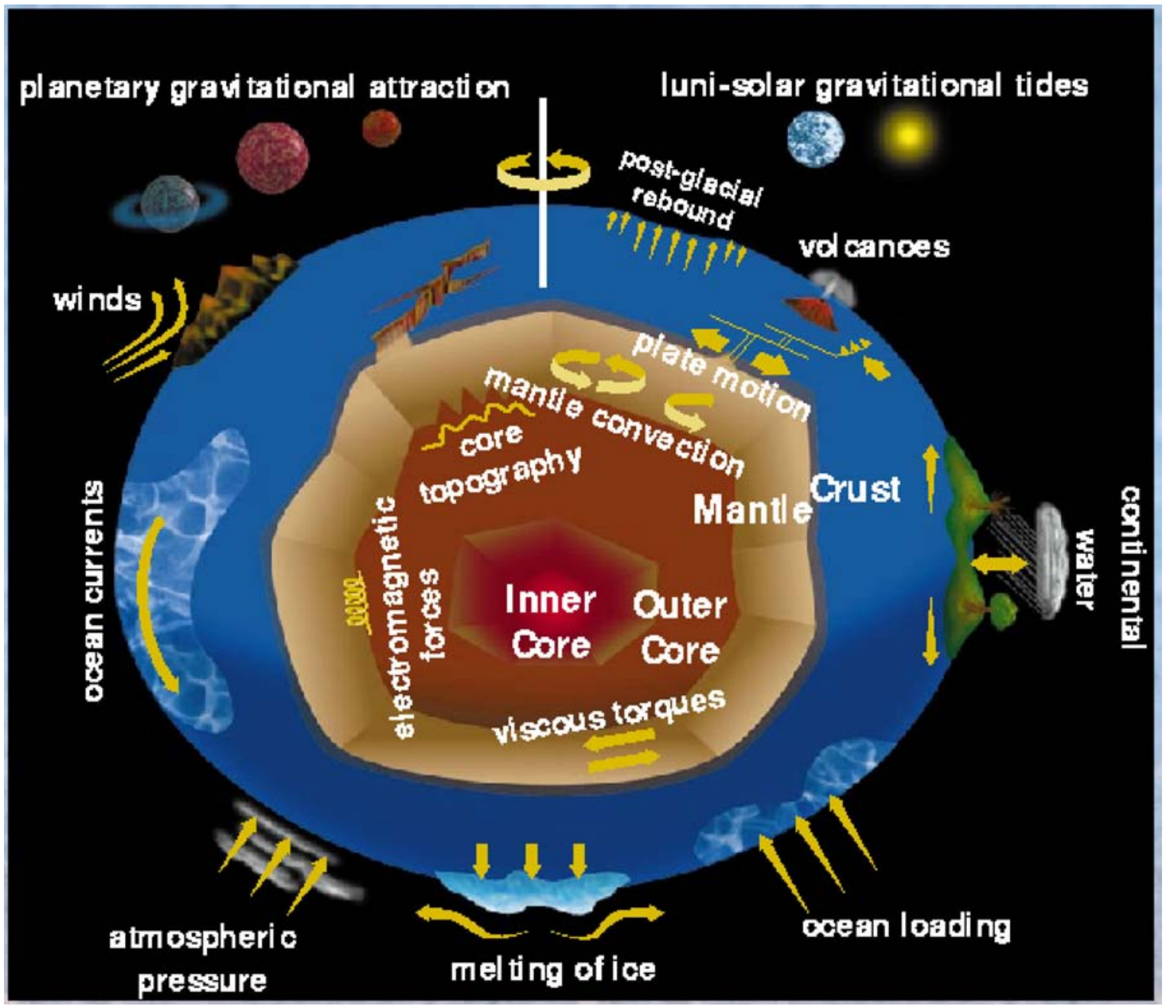

Dynamics of crust and mantle

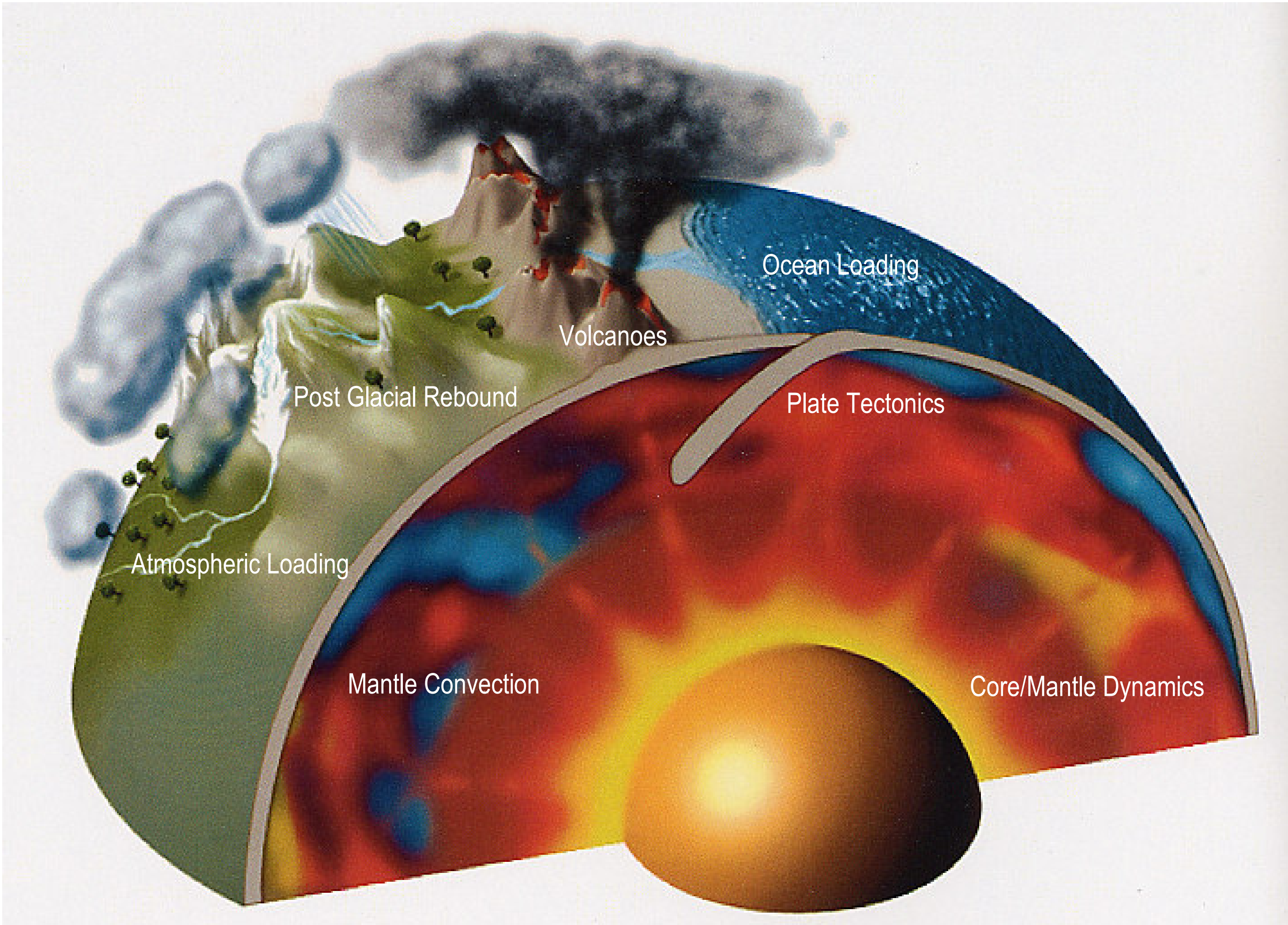

Mass transport phenomena in the upper layers of the Earth

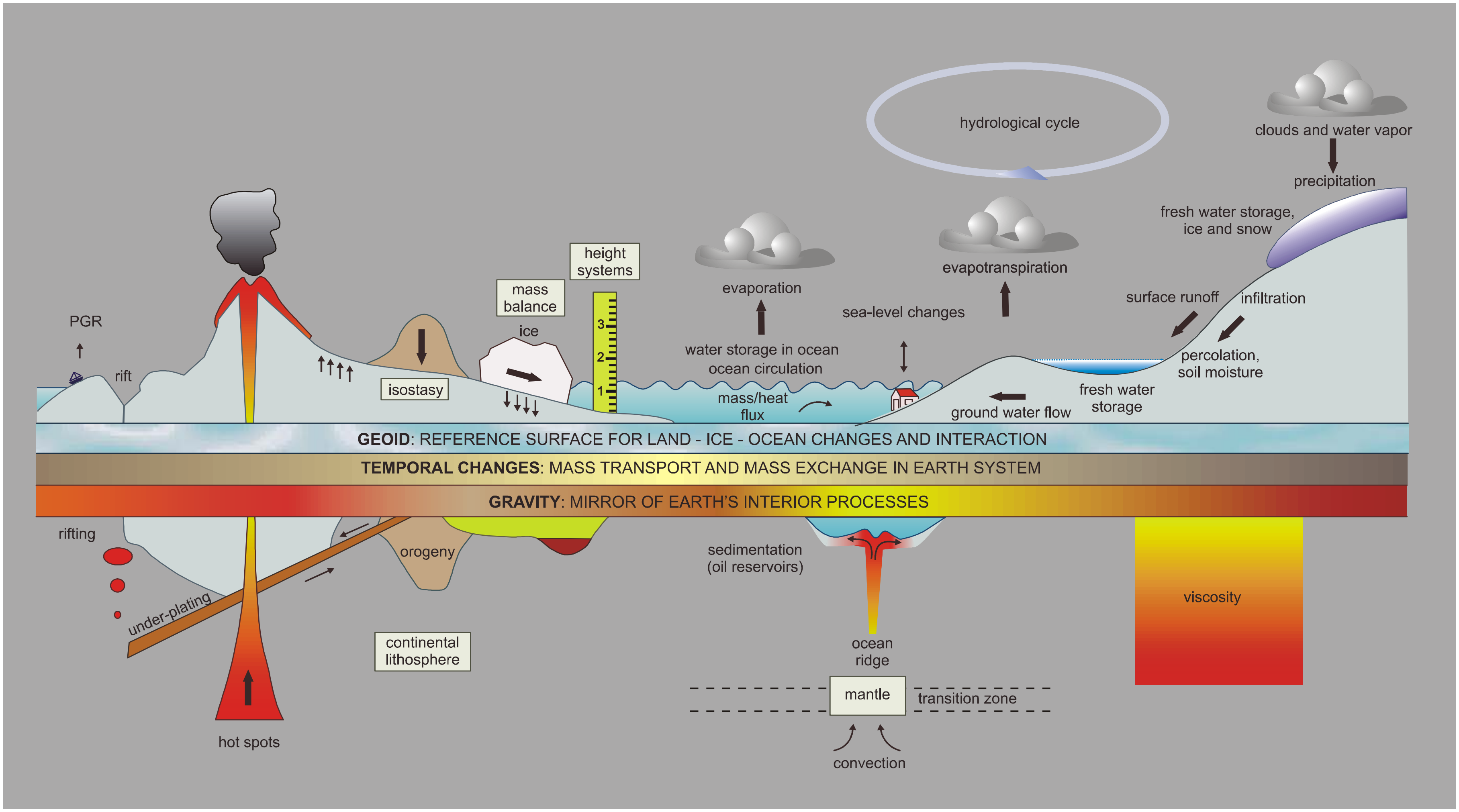

Temporal and spatial resolution of mass transport phenomena

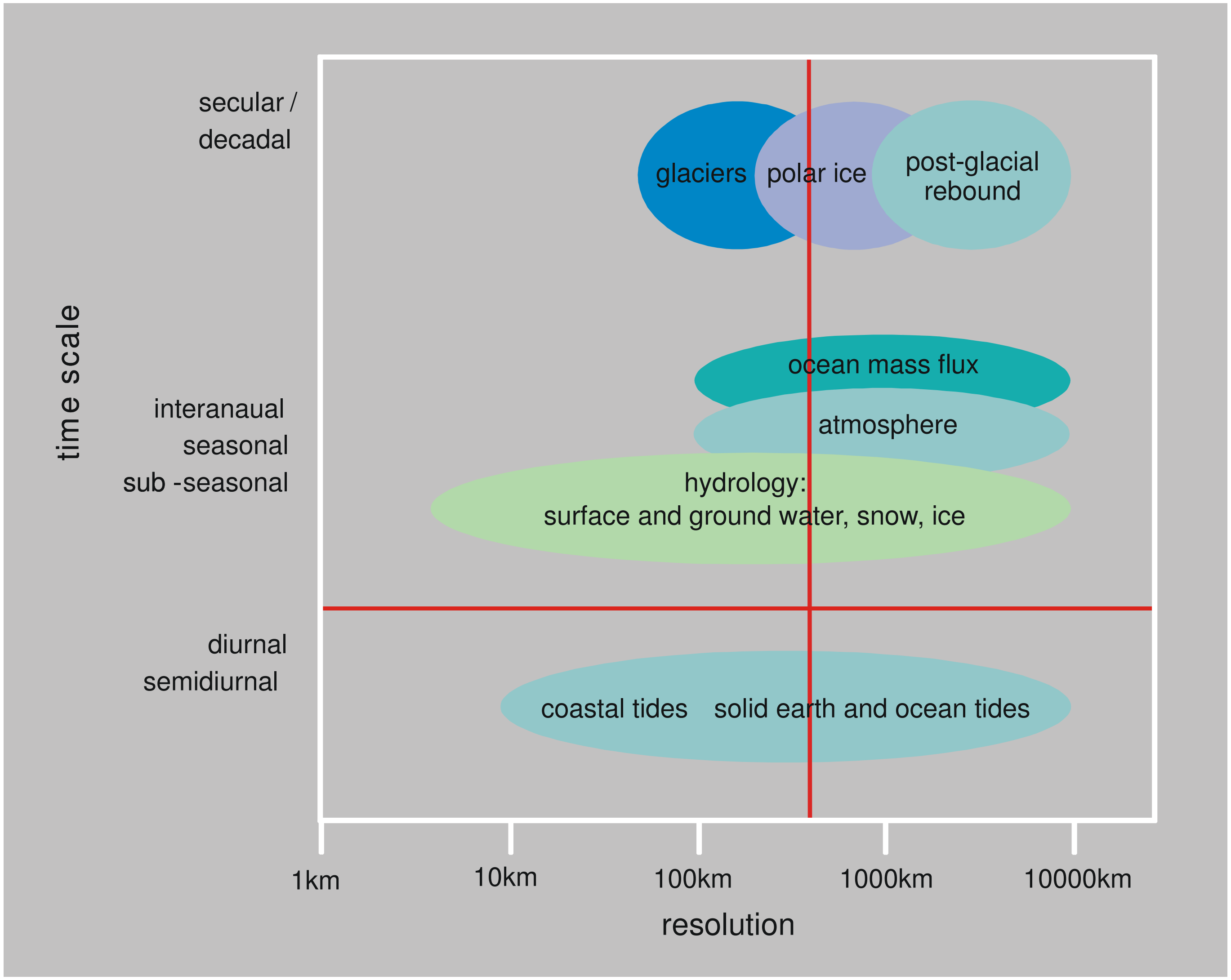

Temporal and spatial resolution of oceanographic features

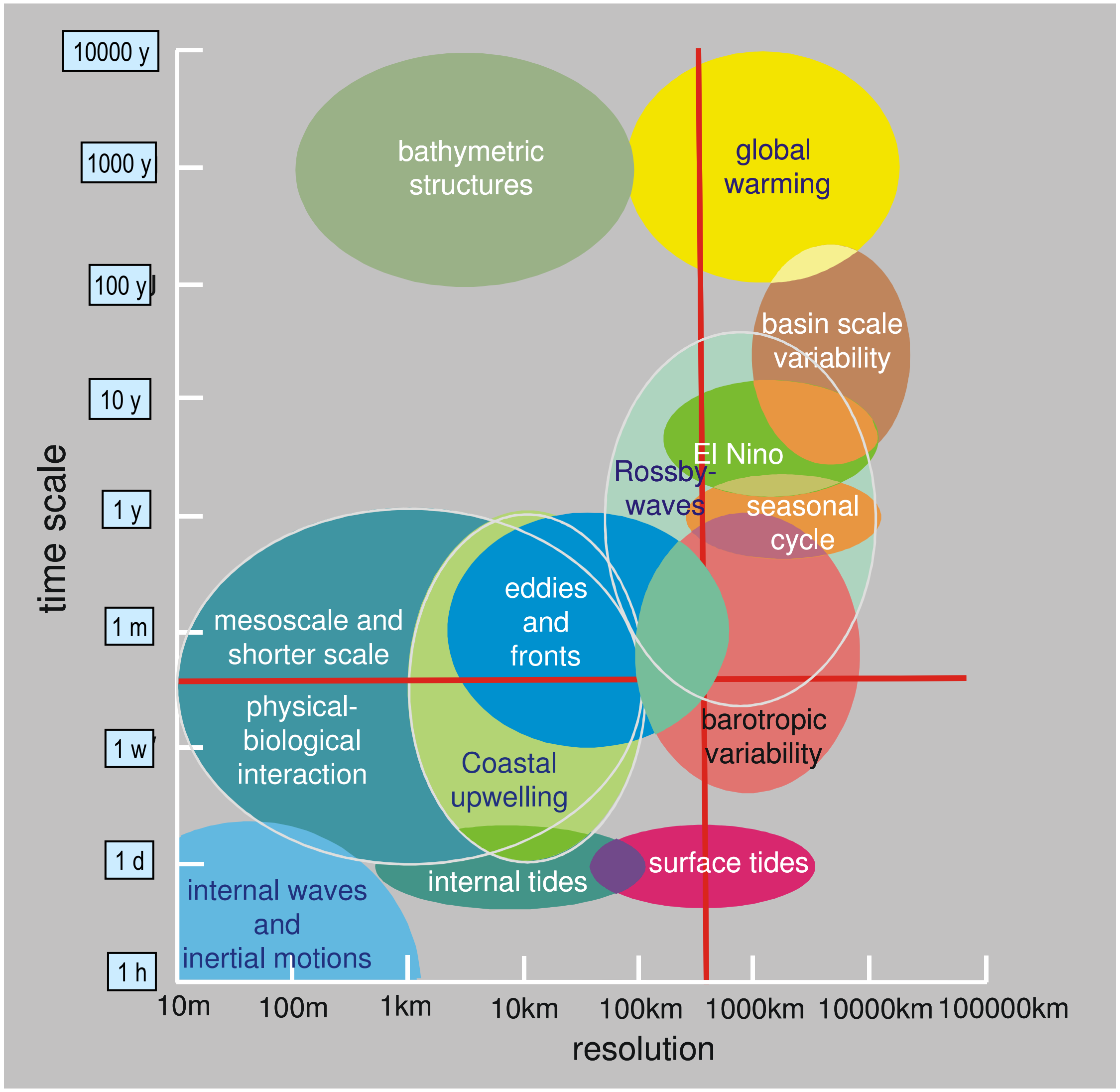

Continental hydrology

Ice mass balance and sea level

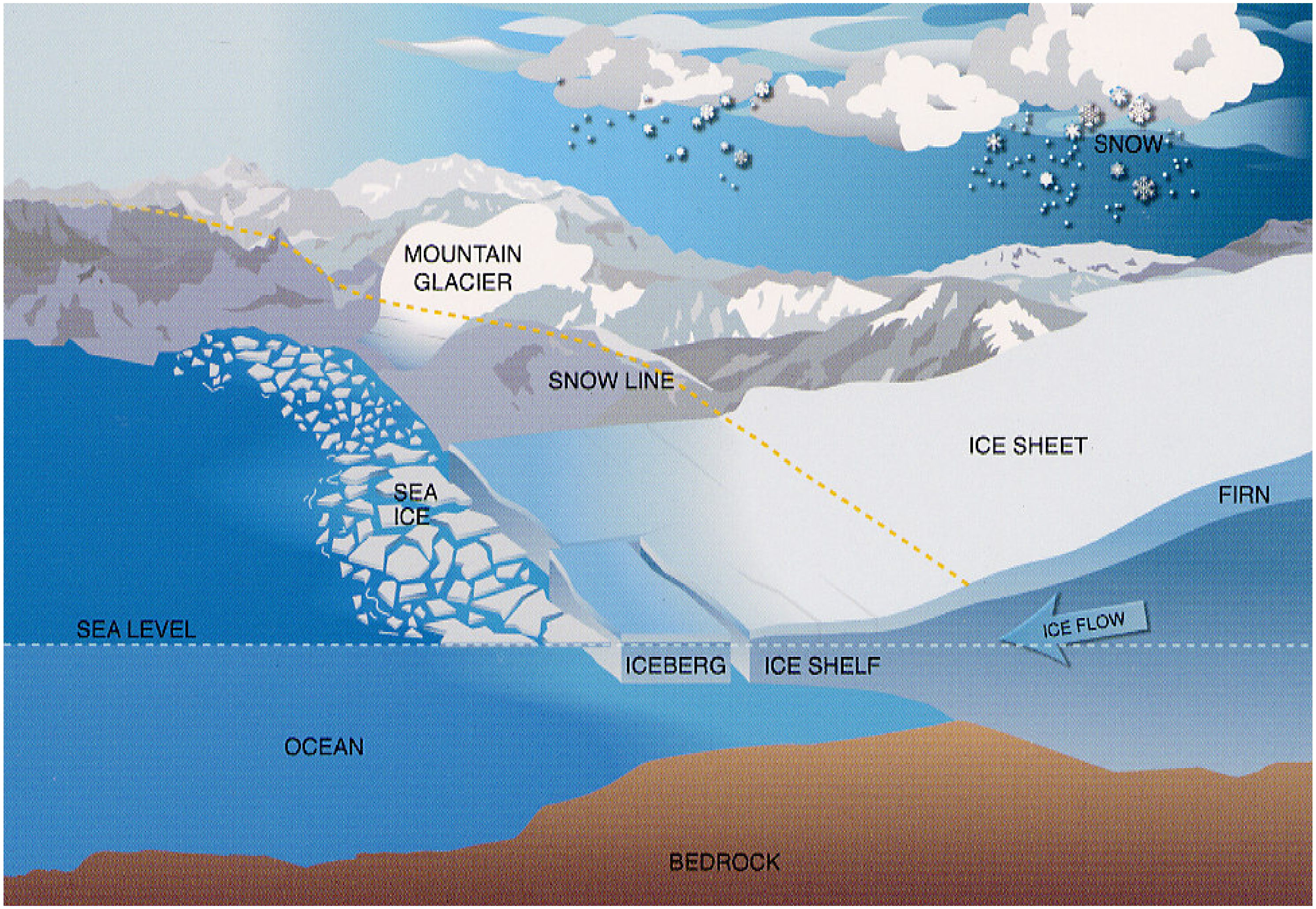

Satellite gravity and altimeter mission products help determine mass transport and mass distribution in a multi-disciplinary environment

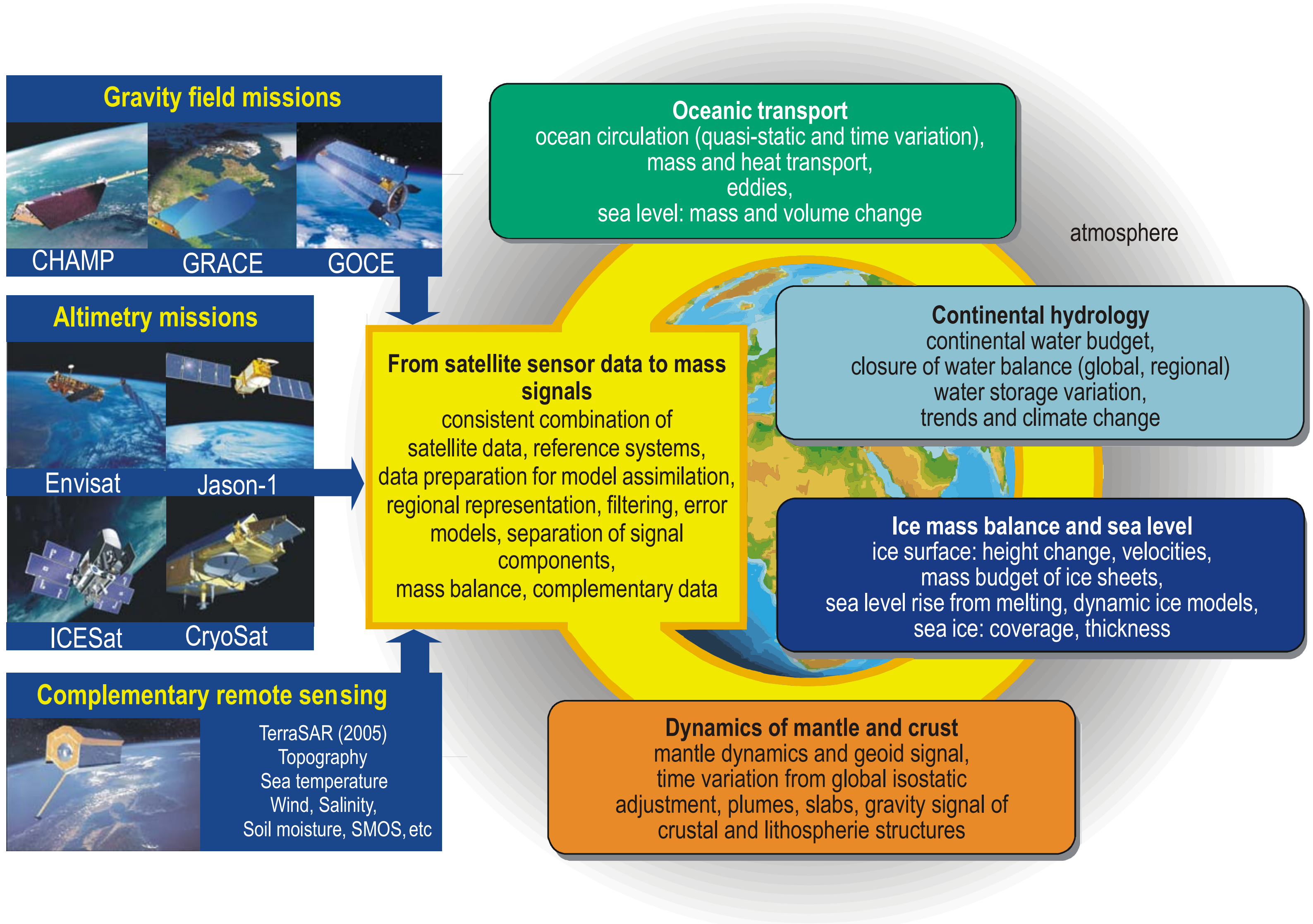

Fundamental questions in Geosciences:

Context for SLR Science:

- What are the causes of the observed global and regional sea level changes?
- What are their relations to the variations in the heat and mass content of the oceans?
- How do the polar ice sheets vary in size and thickness?
- Are there variations in the continental hydrosphere and what are their influences on the climate changes?
- Which geodynamic convective processes cause deformations and motions of the Earth‘s surface?

Mass transport phenomena:

- Hydrological cycle of the continents and in the ice regions,
- Ice mass balance and as a consequence the variation of sea level,
- Mass transport in the oceans, ocean currents transport heat and represent therefore an important factor of climatological development,
- The melting of the large ice covers cause isostatic adjustment,
- Mass changes within the Earth, caused by various forces within the Earth

What is the common tread?

- **The Reference Frame** allows us to connect measurements over:
  - ☞ Time (decades to centuries)
  - ☞ Space (baselines of10’s to 1000’s of kilometers)
  - ☞ Evolving technology
  - ☞ Extendable into Space

- **The Reference Frame** relies on a sufficiently robust ground-based network to provide overall stability on a platform that is moving

What are the geodetic networks?

- The Terrestrial Reference Frame (TRF) is an accurate, stable set of positions and velocities.
- The TRF provides the stable coordinate system that allows us to link measurements over space, time, and evolving technology
- The geodetic networks provide data for determination of the TRF as well as direct science observations.
- GPS, SLR, and VLBI are the three technologies used in the geodetic networks.

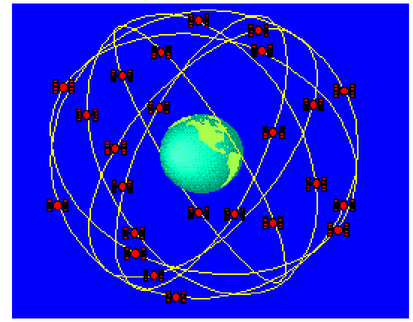

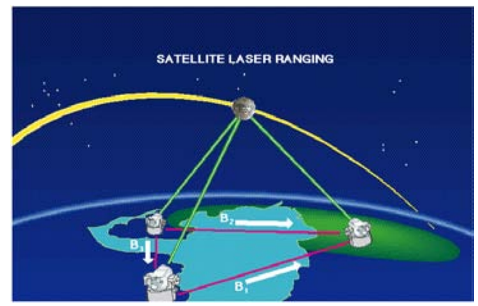

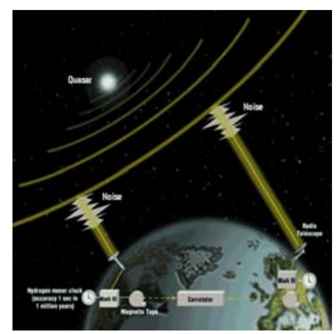

Space Geodesy Techniques

- **VLBI** (Very Long Baseline Interferometry)
- **SLR/LLR** Satellite/Lunar Laser Ranging
- **GNSS** (GPS, GLONASS, future: Galileo)
- **DORIS** (Doppler Orbitography and Radio Positioning Integrated by Satellite)

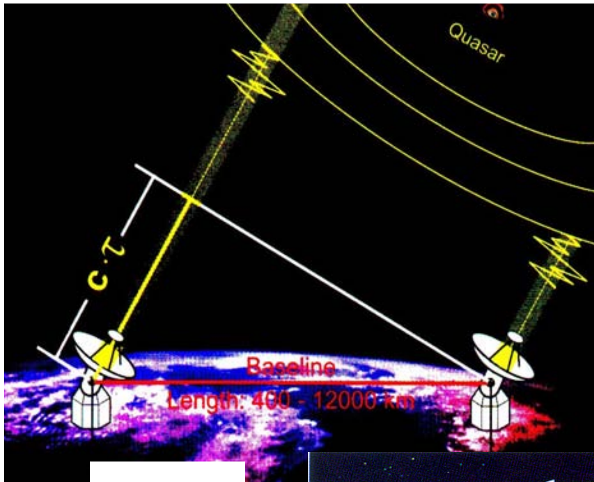

VLBI

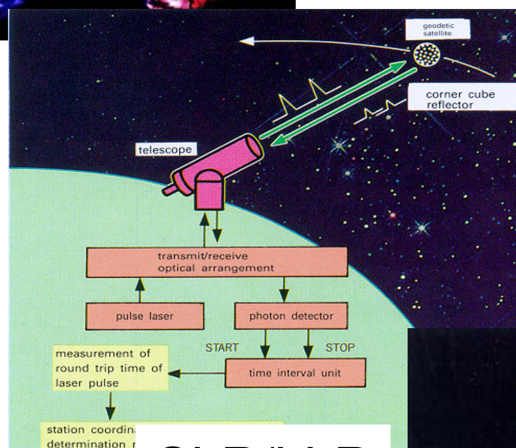

SLR/LLR

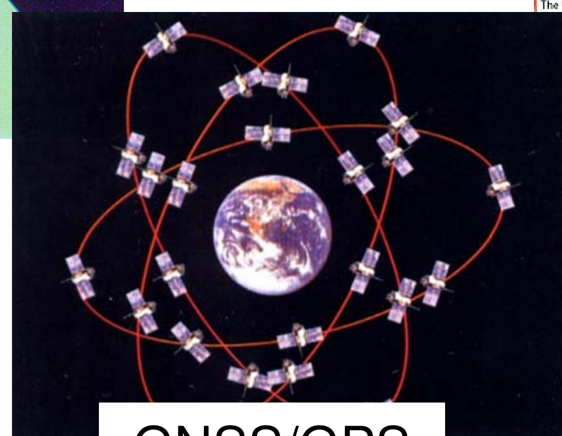

GNSS/GPS

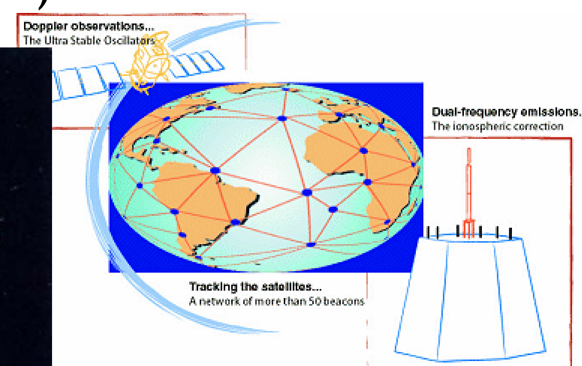

DORIS

Satellite Laser Ranging Technique

Precise range measurement between an SLR ground station and a retroreflector- equipped satellite using ultrashort laser pulses corrected for refraction, satellite center of mass, and the internal delay of the ranging machine.

- Simple range measurement
- Space segment is passive
- Simple refraction model
- Night / Day Operation
- Near real-time global data availability
- Satellite altitudes from 400 km to 20,000 km (e.g. GPS/GLONASS), and the Moon
- Cm. satellite Orbit Accuracy
- Able to see small changes by looking at long time series

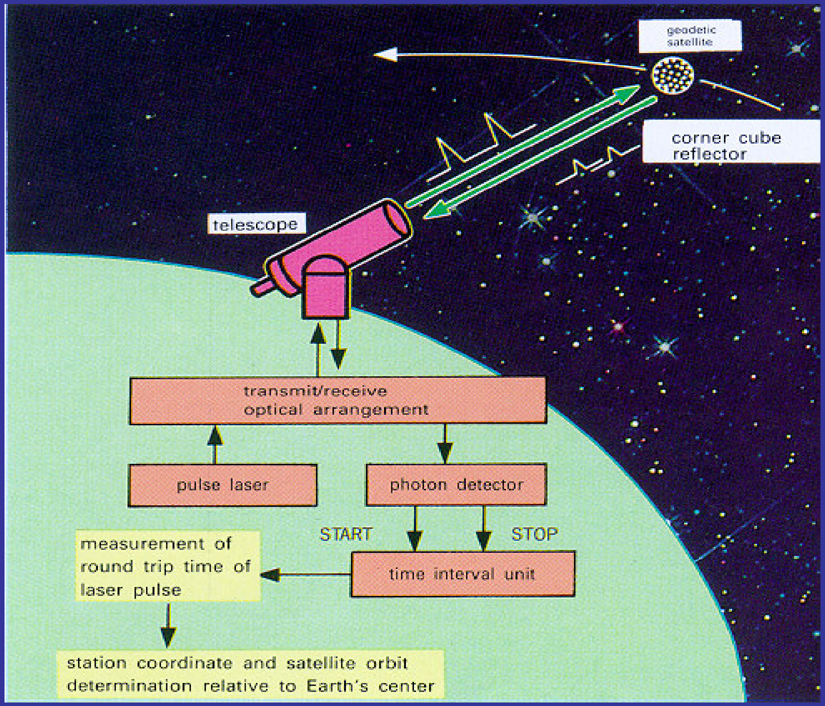

- **Unambiguous centimeter accuracy orbits**
- **Long-term stable time series**

SLR Science and Applications

- Measurements
  - Precision Orbit Determination (POD)
  - Time History of Station Positions and Motions
- Products
  - Terrestrial Reference Frame (Center of Mass and Scale)
  - Plate Tectonics and Crustal Deformation
  - Static and Time-varying Gravity Field
  - Earth Orientation and Rotation (Polar Motion, length of day)
  - Orbits and Calibration of Altimetry Missions (Oceans, Ice)
  - Total Earth Mass Distribution
  - Space Science - Tether Dynamics, etc.
  - Relativity
- More than 60 Space Missions Supported since 1970
- Four Missions Rescued in the Last Decade

Sample of SLR Satellite Constellation

(Geodetic Satellites)

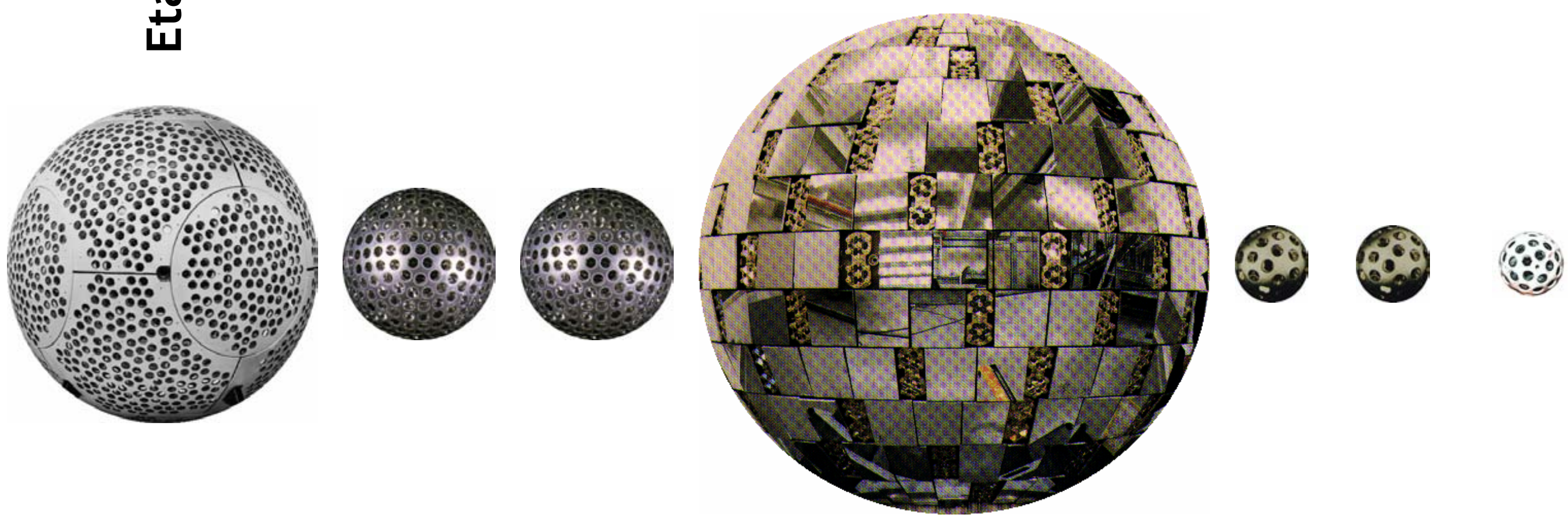

	Etalon-I & -II	LAGEOS-I	LAGEOS-II	Ajisai	Starlette	Stella	GFZ-1
Inclination	64.8°	109.8°	52.6°	50°	50°	98.6°	51.6°
Perigee ht. (km)	19,120	5,860	5,620	1,490	810	800	396
Diameter (cm)	129.4	60	60	215	24	24	20
Mass (kg)	1415	407	405.4	685	47.3	47.3	20.6

Sample of SLR Satellite Constellation

(POD Support)

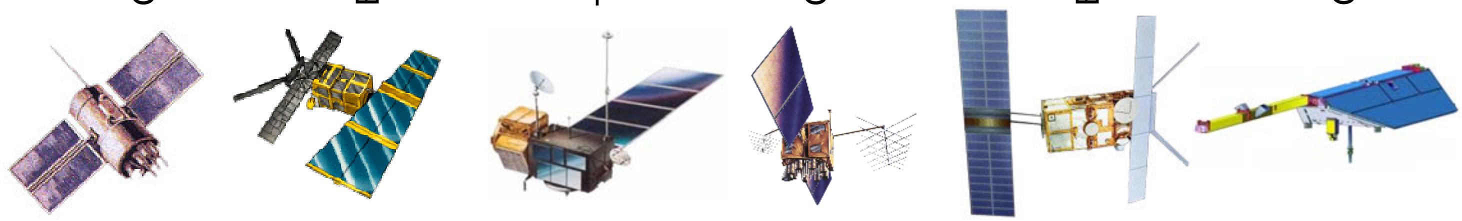

	GLONASS	ERS-1	TOPEX	GPS	ERS-2	CHAMP
Inclination	64°	98.5°	66°	55°	98.6°	87.27°
Perigee ht. (km)	19,140	780	1,350	20,100	800	474
Mass (kg)	1,400	2,400	2,400	930	2,516	400

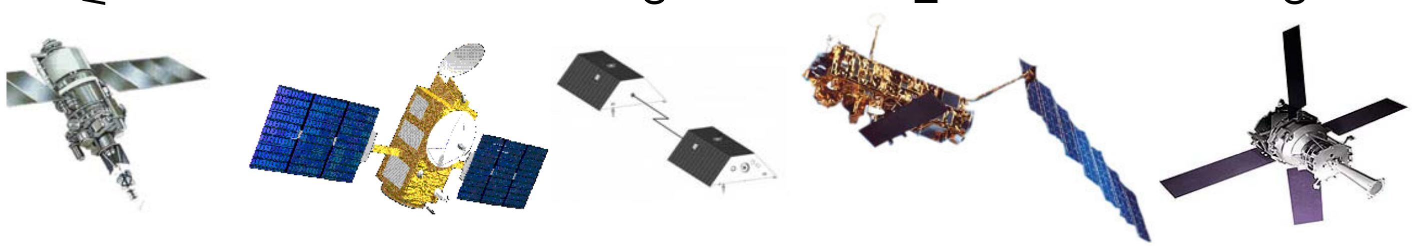

	Meteor-3M	Jason-1	GRACE	Envisat	GP-B
Inclination	99.64°	66°	89°	98.5°	90°
Perigee ht. (km)	1,019	1,336	450	800	650
Mass (kg)	5,500	500	432/sat.	8,211	3,334

Example Satellite Configurations

GRACE

(courtesy of U. TX/CSR)

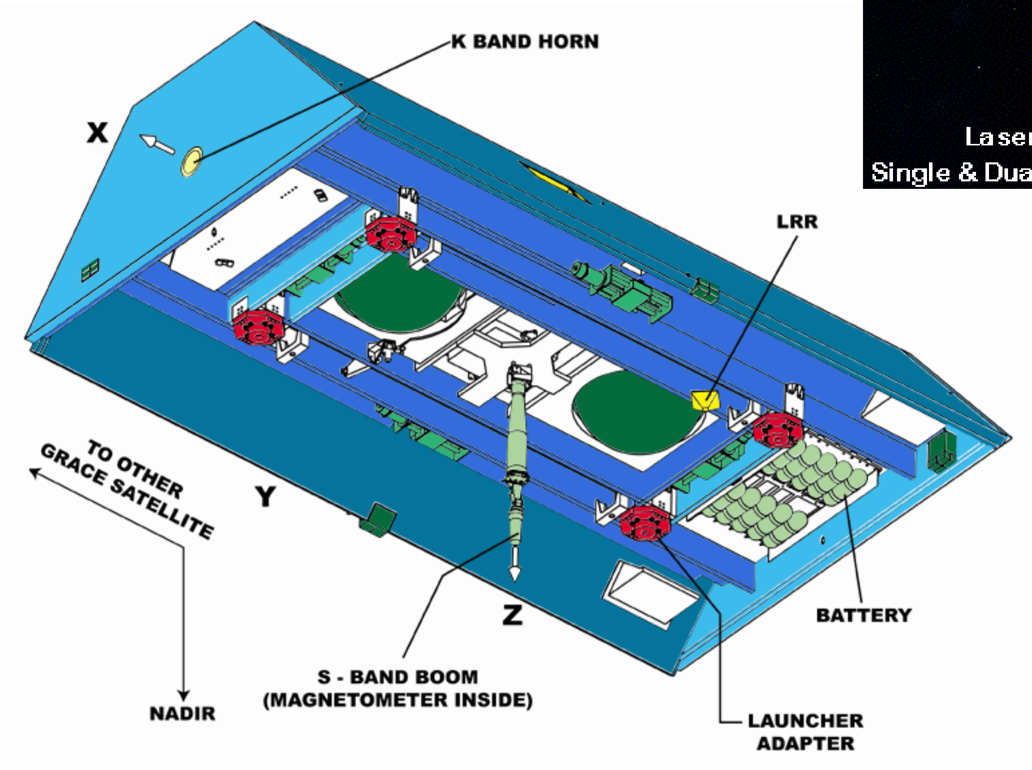

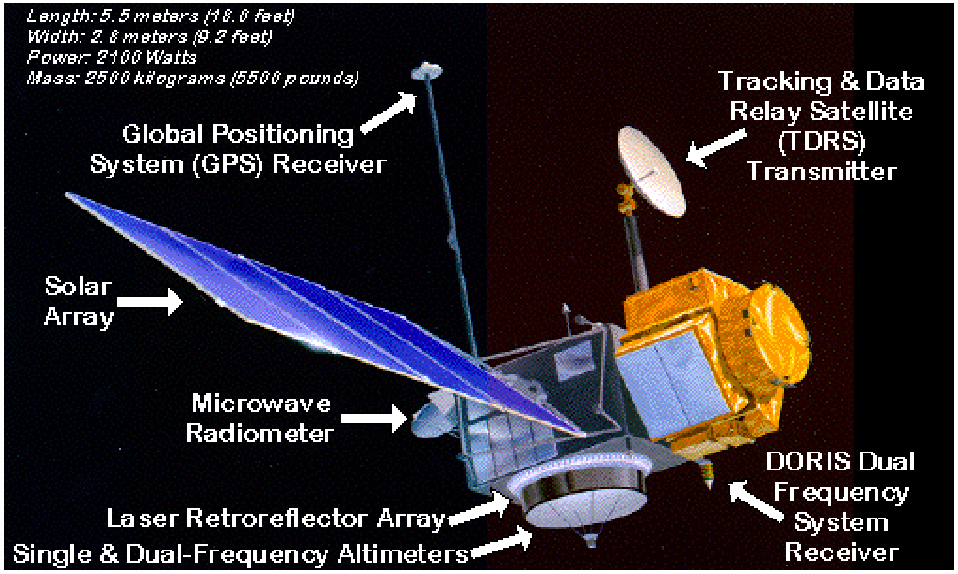

TOPEX/Poseidon

Lageos-1 and -2 global rms for all 10 day arcs

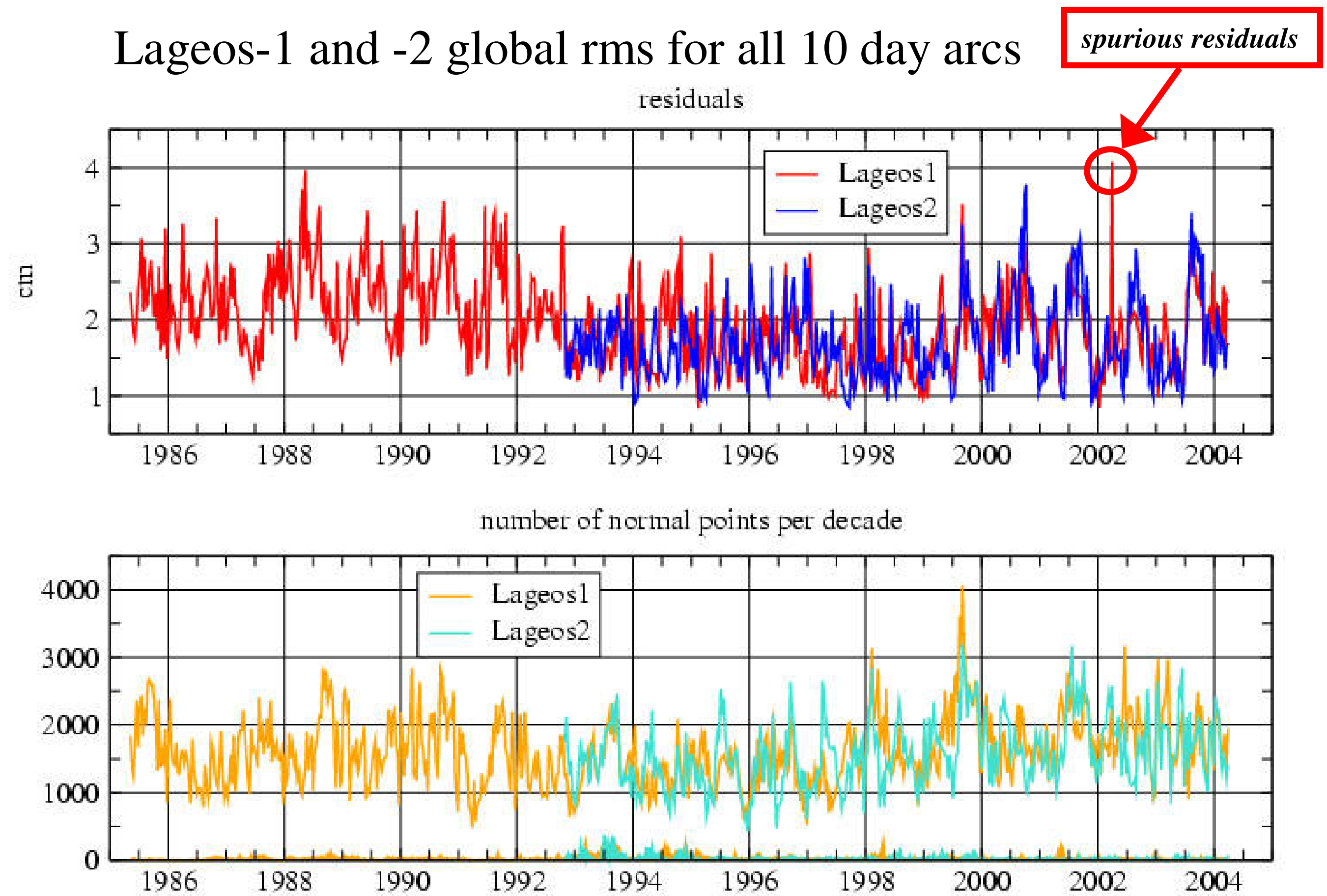

GEOCENTER MOTION

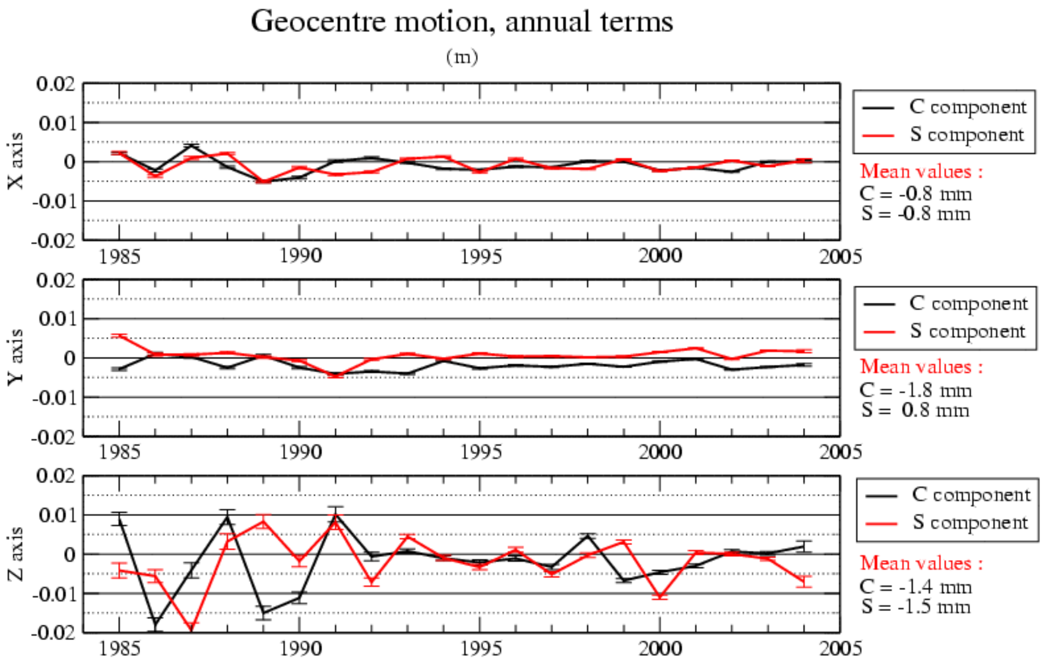

<u>Mean annual terms amount to :</u>

1.2 mm in X, with a minimum in February

2.0 mm in Y, with a minimum in December

1.8 mm in Z, with a minimum in February

- mm-level Geodesy requires understanding of the reference frame and its distortions to acute levels of precision.
- Shown here is the change in the origin of the crust-fixed frame w.r.t. the center of mass due to non tidal mass transport in the atmospheric and hydrospheric systems.

Mean Sea Surface

from an Integrated and Calibrated Suite of Satellite Altimeters

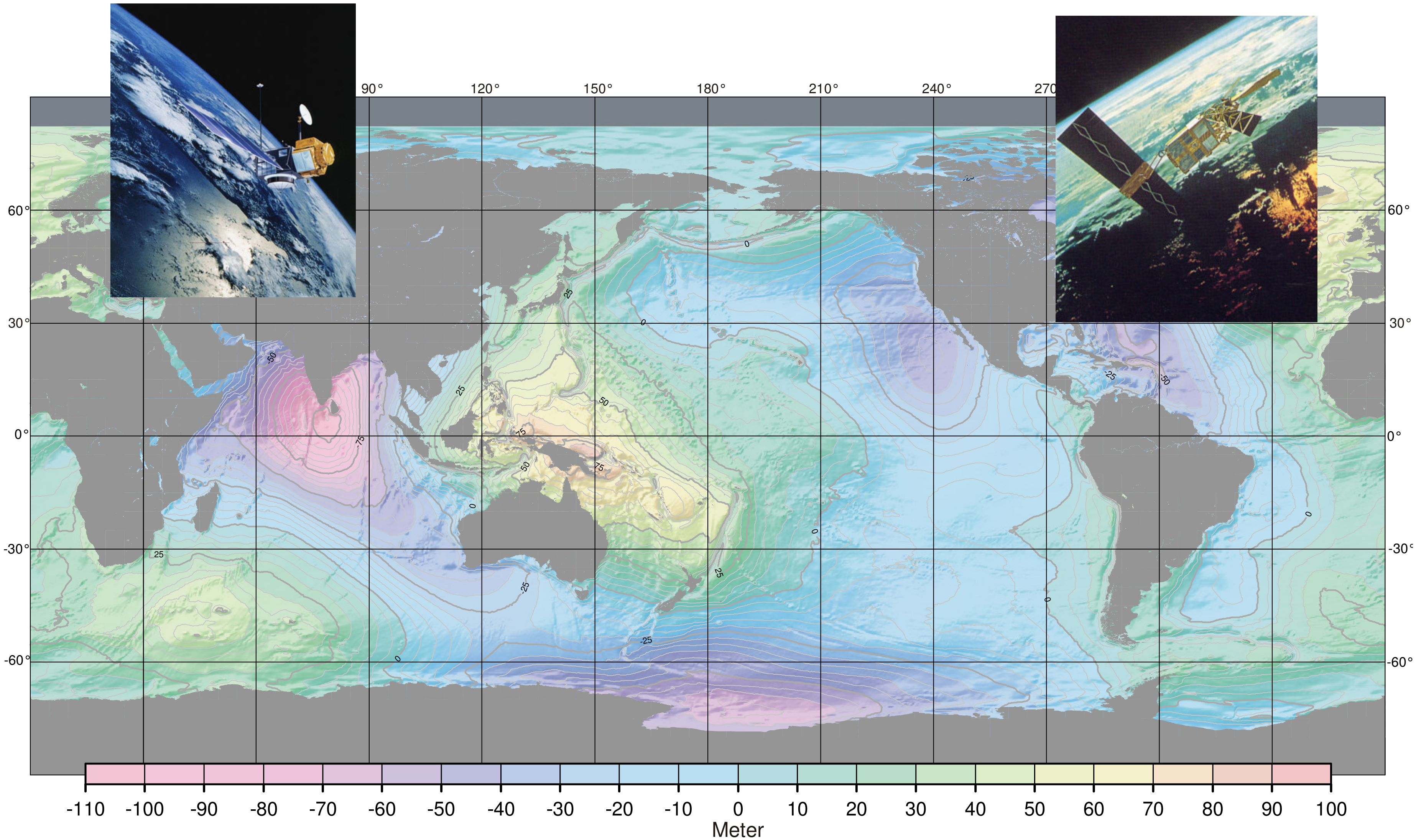

Rise in Sea Level

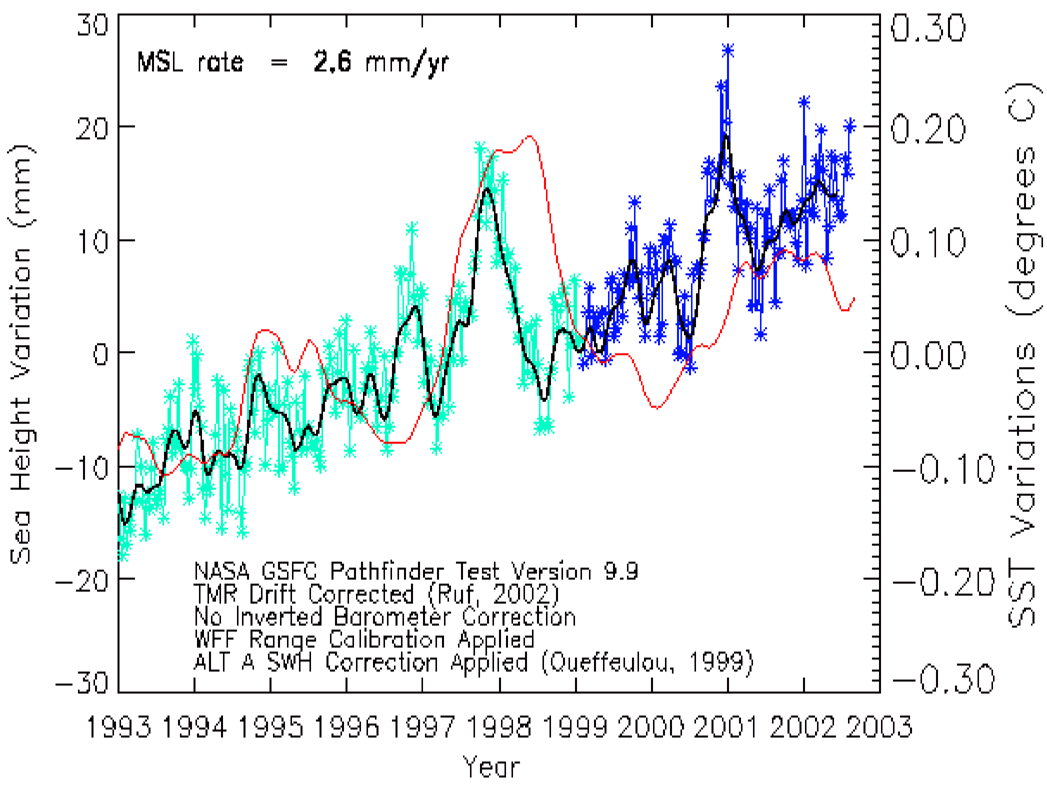

Gravity Field Model

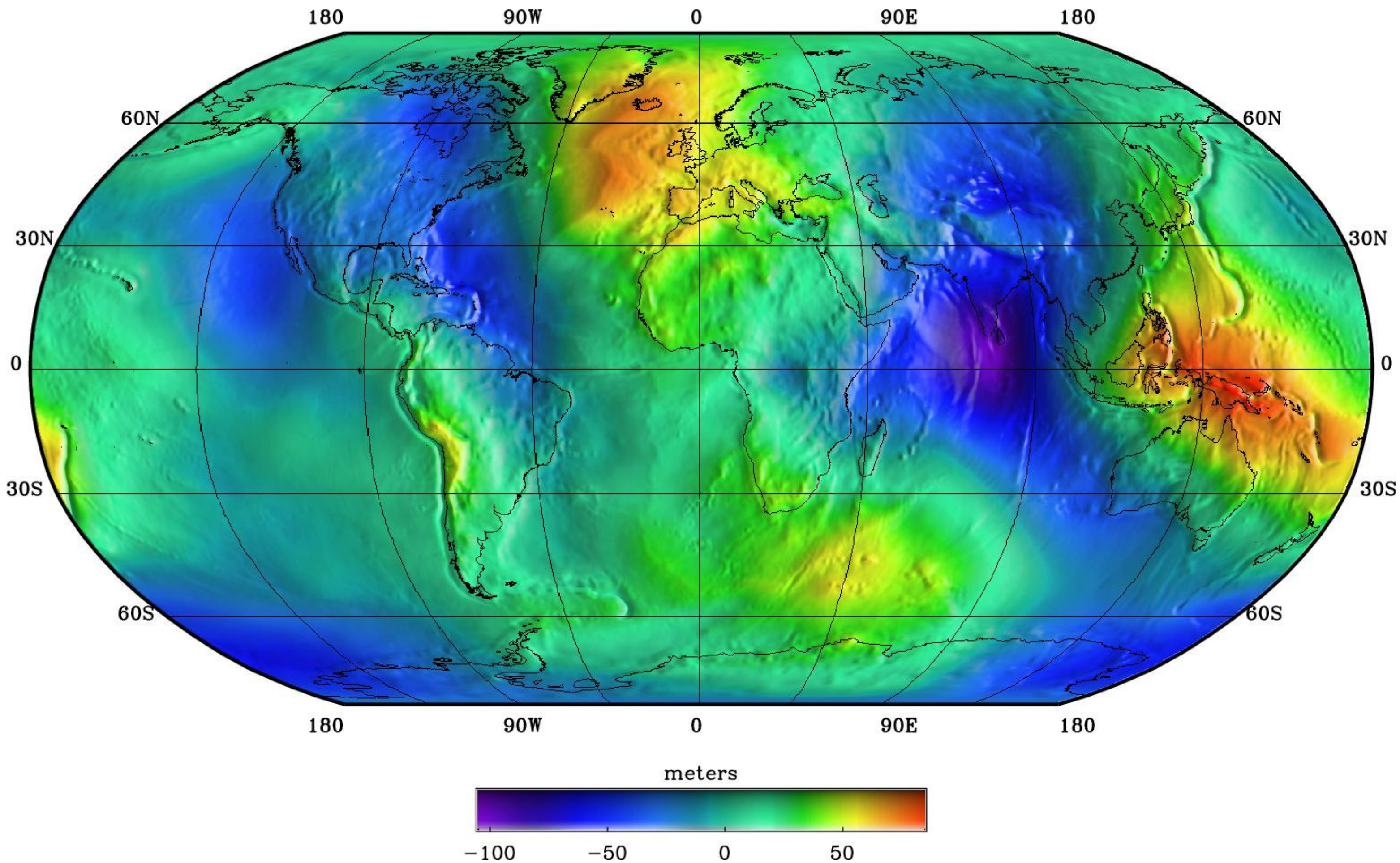

Reduction in Major SLR Error Source: GRACE Gravity Field Modeling

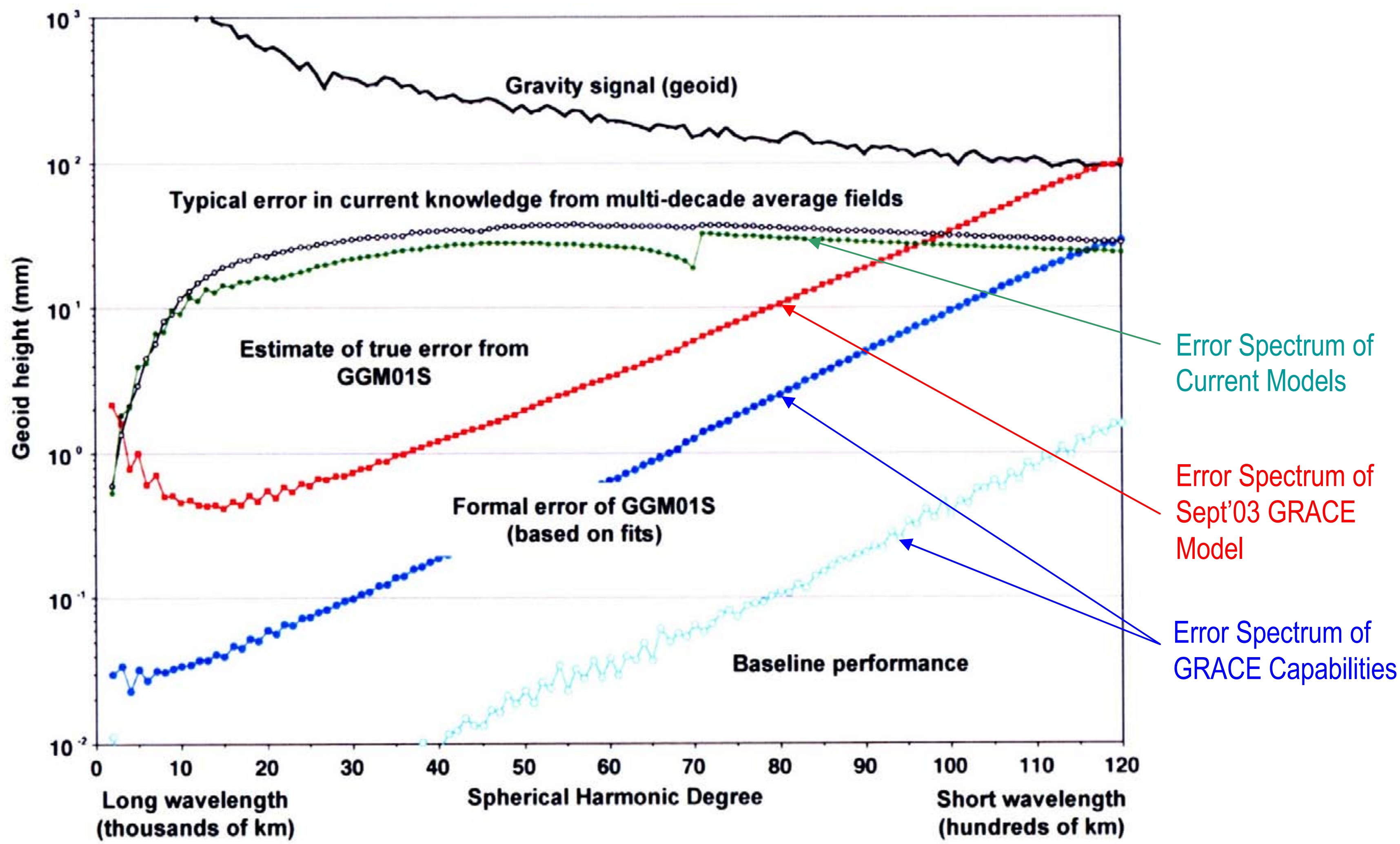

Time Varying Gravity:
A Unique Form of Remote Sensing

REPORTS

29. D. R. Jennison, A. Bogicevic, Surf. Sci. Lett. 464, 108 (2000).
30. A. E. Mattsson, D. R. Jennison, in preparation.
31. L. A. Curtiss, K. Raghavachari, G. W. Trucks, J. A. Pople, J. Chem. Phys. 94, 7221 (1991).
32. The endothermic reaction $2OH^- + Co^0 \rightarrow O^{2-}Co^{2+} + H_2O$ does not produce Co(II).
33. G. Mills, H. Jonsson, G. K. Schenter, Surf. Sci. 324, 305 (1995).
34. The LDA binding energy (1.08 eV) is likely below the real value (28). Estimating the surface self-energy correction (30) produces this estimate. In addition, the thermal energy of the source contributes 0.11 eV.
35. J. Strömquist et al., Surface Science, 397, 382 (1998).
36. M. Persson et al., J. Chem. Phys. 110, 2240 (1999).
37. K. C. Hass, W. F. Schneider, A. Curioni, W. Andreoni, J. Phys. Chem. B 104, 5527 (2000).

38. We thank R. R. Stumpf for critical comments and J. Strömquist for useful discussions. Pacific Northwest National Laboratory (PNNL) and Sandia National Laboratory (SNL) are multiprogram laboratories operated for the U.S. Department of Energy by Battelle Memorial Institute under Contract DE-AC06-76RLO 1830 (PNNL), and by Sandia Corporation, a Lockheed Martin Company, under Contract DE-AC04-94AL85000 (SNL). The experimental work was conducted in the Environmental Molecular Sciences Laboratory, a national scientific user facility sponsored by the Department of Energy's Office of Biological and Environmental Research and located at PNNL. T.R.M. acknowledges the Motorola/SNL computational materials Cooperative Research and Development Agreement. S.A.C. and T.D. were supported by the U.S. Department of Energy, Office of Science, Office of Basic Energy Sciences, Division of Materials Science at PNNL.

30 April 2002; accepted 14 June 2002

Detection of a Large-Scale Mass Redistribution in the Terrestrial System Since 1998

Christopher M. Cox[1]* and Benjamin F. Chao[2]

Earth's dynamic oblateness (J_2) had been undergoing a decrease, according to space geodetic observations over the past 25 years, until around 1998, when it switched quite suddenly to an increasing trend that has continued to the present. The secular decrease in J_2 resulted primarily from the postglacial rebound in the mantle. The present increase, whose geophysical cause(s) are uncertain, thus signifies a large change in global mass distribution with a J_2 effect that considerably overshadows that of mantle rebound.

Earth's mean tide-free dynamic oblateness $(J_2) \equiv [C - (A + B)/2]/MR^2 = 1.082627 \times 10^{-3}$, where $C > B \geq A$ are Earth's mean principal moments of inertia and M and R are the mean mass and radius, respectively. Satellite laser ranging (SLR) has yielded precise determination of the temporal variation in the low-degree spherical harmonic components of Earth's gravity field, beginning with the initial observations of J_2 change made by observing Lageos-1 satellite orbital node accelerations (1, 2). More recent studies have extended the knowledge to higher degree zonals and examined the annual signals in the low-degree geopotential (3–5). The estimated values of the J_2 rate have ranged from -2.5×10^{-11} year^{-1} to -3×10^{-11} year^{-1}.

The extension of comprehensive solutions for low-degree geopotential zonal, static, annual, and rate terms and the 9.3- and 18.6-year ocean tide amplitudes to include data since 1997 has resulted in increasingly significant changes in the estimated J_2 rate and 18.6-year tide amplitude (4). These changes implied that the models for these terms were not accommodating the observed signal. Consequently, we estimated a time series of low-degree (maximum degree of 4) static geopotential solutions using SLR observations of 10 satellites over the period from 1979 to 2002. The inclusion of multiple orbital inclinations improves separation of the higher degree zonal components and allows recovery of the gravity coefficients over shorter time periods. All processing used the same algorithms used to develop the EGM96S satellite-only gravity model and to calibrate that model's covariance (5). The 18.6-year and much smaller 9.3-year tide amplitudes were set to the values estimated in the comprehensive solution with data from 1979 through 1997 (4). The applied 18.6-year tide amplitude of 1.41 cm has the equivalent J_2 amplitude of 1.67×10^{-10}. The 18.6-year tide–J_2 effect is minimized (that is, the geopotential is less oblate) when the lunar node is 0 degrees, which occurred in mid-October 1987.

Shown in Fig. 1 is the estimated J_2 as a function of time, $J_2(t)$. Lageos-1 data are present throughout, and Starlette data are present from January 1980 onward. Data completeness issues precluded the use of the earlier Starlette and Lageos-1 data. Other satellites were added when launched: Ajisai from August 1986 and Lageos-2 and several other satellites from 1992 onward. TOPEX/POSEIDON (T/P), which is also tracked by the Détermination d'Orbite et Radiopositionnement Intégrés par Satellite system, was added in January 1993. The formal uncertainties shown reflect the SLR data weights derived from the calibration of the comprehensive 19-year solution and should be realistic (6).

Dominant in $J_2(t)$ is a seasonal signal of amplitude 3.2×10^{-10}, which is driven by meteorologic mass redistribution in the atmosphere-hydrosphere-cryosphere system (7–10). Also plotted in Fig. 1 is the atmospheric contribution calculated according to the National Center for Environmental Prediction (NCEP) reanalysis data (11), including the inverted-barometer (IB) correction (12). Subtraction of this signal and further empirical removal of the residual seasonal signals (which are attributable to the poorly known seasonal mass redistribution in the oceans and land hydrology) result in a nonatmospheric and nonseasonal $J_2(t)$ (Fig. 2).

A linear fit to the observed J_2 through 1996 shows a decrease in J_2 of -2.8×10^{-11} year^{-1} (Fig. 2). For this period, the uncertainty for the J_2 rate in the comprehensive solution (which considers the correlation with the 18.6-year tide) is 0.4×10^{-11} year^{-1}. Despite the lack of data before 1979, the results are in excellent agreement with estimates of the J_2 rate that included those data (2). The secular drift results primarily from postglacial rebound (PGR) (2, 13, 14) in the mantle, plus various secondary contributions of climatic and anthropogenic origin (for example, reservoirs, which are an order of magnitude too small to explain the recent observations) (4, 15, 16). At some time during 1997 or 1998, the trend reversed. The post-1996 points have deviated from the pre-1997 slope by about six times the uncertainties, on average, over that period. A linear fit from 1997 onward yields a rate of $+2.2 \times 10^{-11}$ year^{-1}. On the basis of the comprehensive solutions, the uncertainty for this rate is $\sim 0.7 \times 10^{-11}$ year^{-1}; however, because of the nonlinearity in $J_2(t)$, the slope can vary by more than the uncertainty value, depending on the period fitted. Another departure may exist around 1980, but excepting a few data points the deviation is only one to two times the uncertainties, making the importance unclear.

An increase in J_2 means a net transport of mass from high to low latitude (the nodal lines of J_2 are $\pm$ 35.3° latitude). Transport of terrestrial water and/or ice mass to the oceans is one likely cause, because most of the ice mass resides in high-latitude polar caps and glaciers. As an example of the mass flux involved, imagine one fictitious scenario that

[1]Raytheon Information Technology and Scientific Services (ITSS). [2]Space Geodesy Branch, NASA Goddard Space Flight Center, Code 926, Greenbelt, MD 20771, USA.

*To whom correspondence should be addressed. E-mail: ccox@stokes.gsfc.nasa.gov

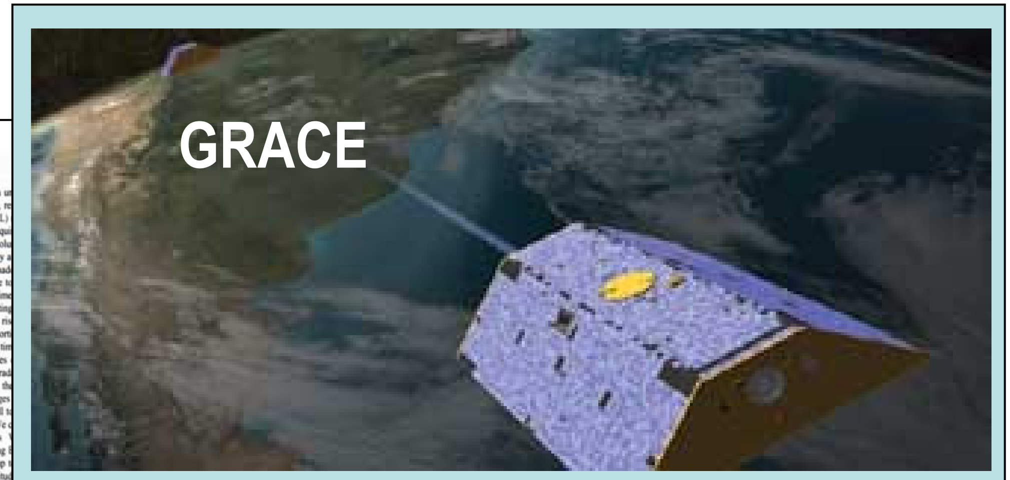

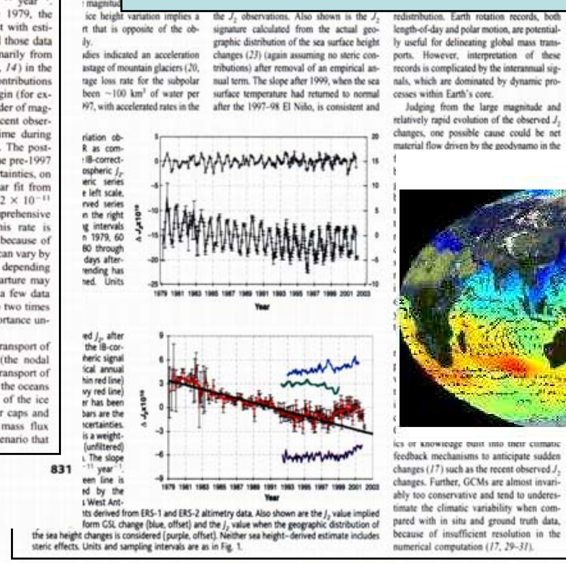

Year

Year

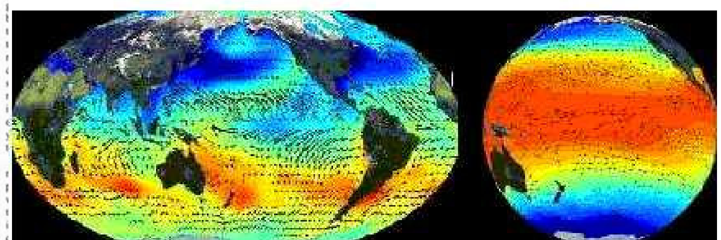

Geodetic Networks: Monitoring Temporal Gravity Changes Using SLR

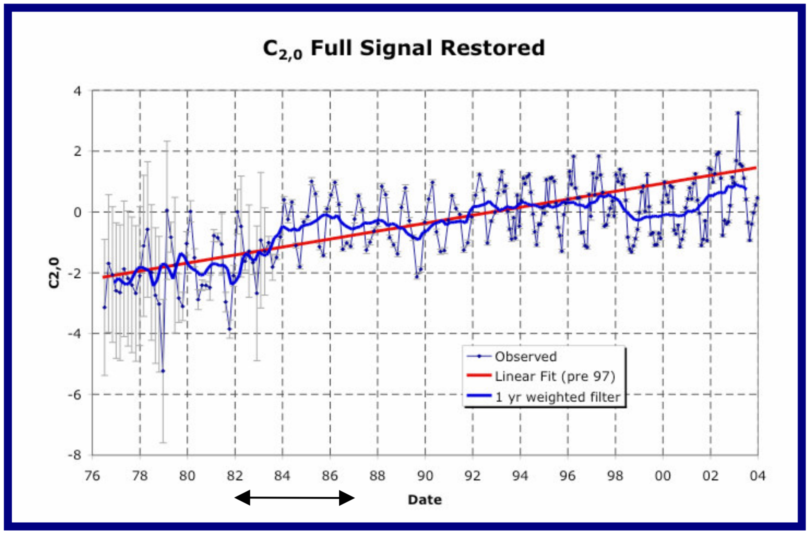

Duration of GRACE

- +0.6 correlation between $S_{2,2}$ time series and the SOI when $S_{2,2}$ is shifted forward in time by 12 months.
- Evidence of El Nino prediction?
- Reported by Cox, Chao et al. (AGU, 2003)

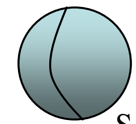

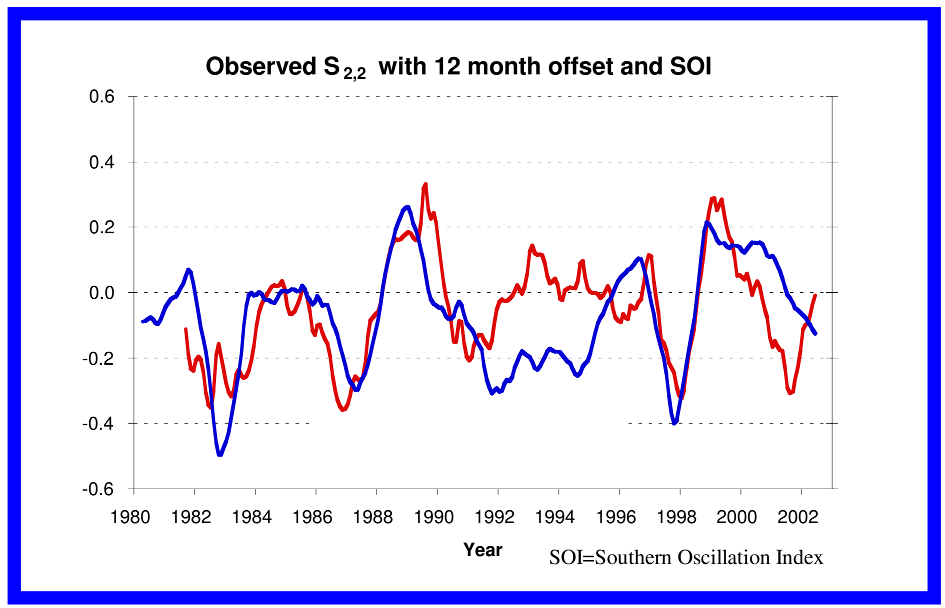

SOI=Southern Oscillation Index

- Anomalistic behavior of J_2 time series
- First detection of large-scale unanticipated mass redistribution
- Reported by Cox and Chao, (SCIENCE, 2002)

Post glacial rebound

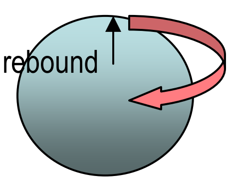

Unexpected SLR 1998+ results

Reflector Satellite

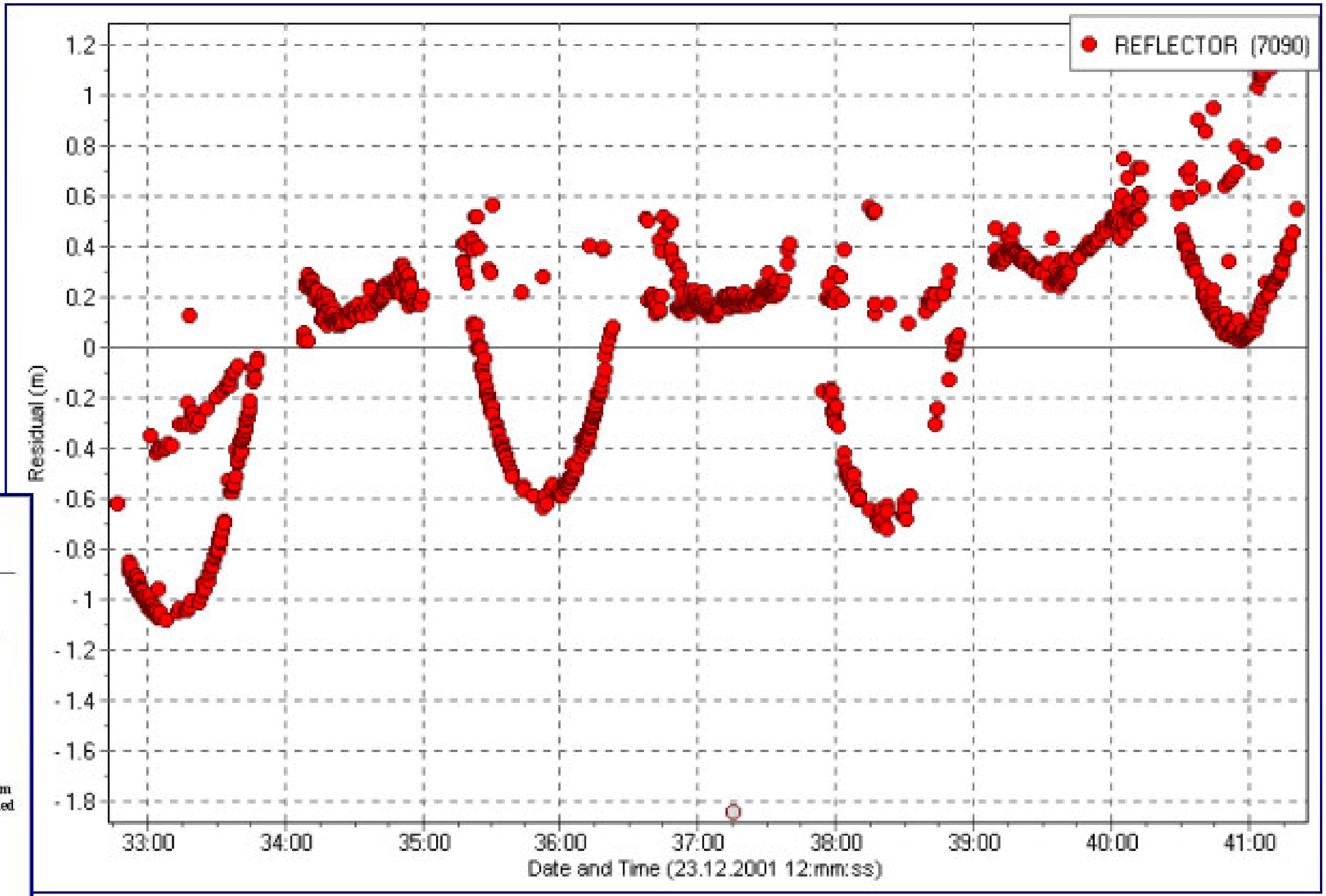

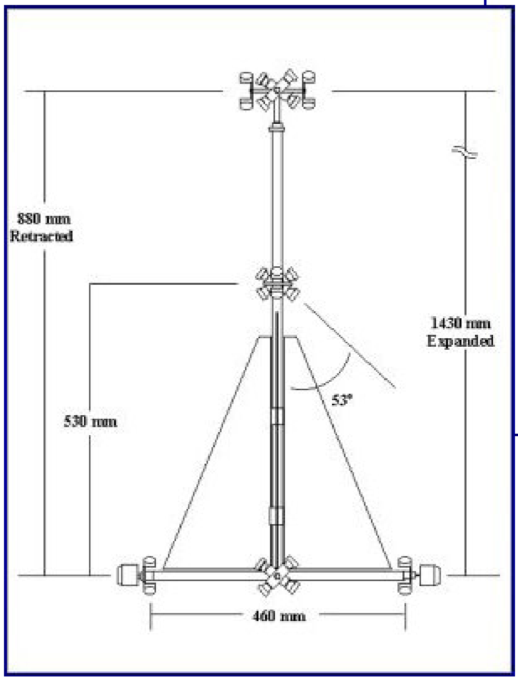

SLR Network Map

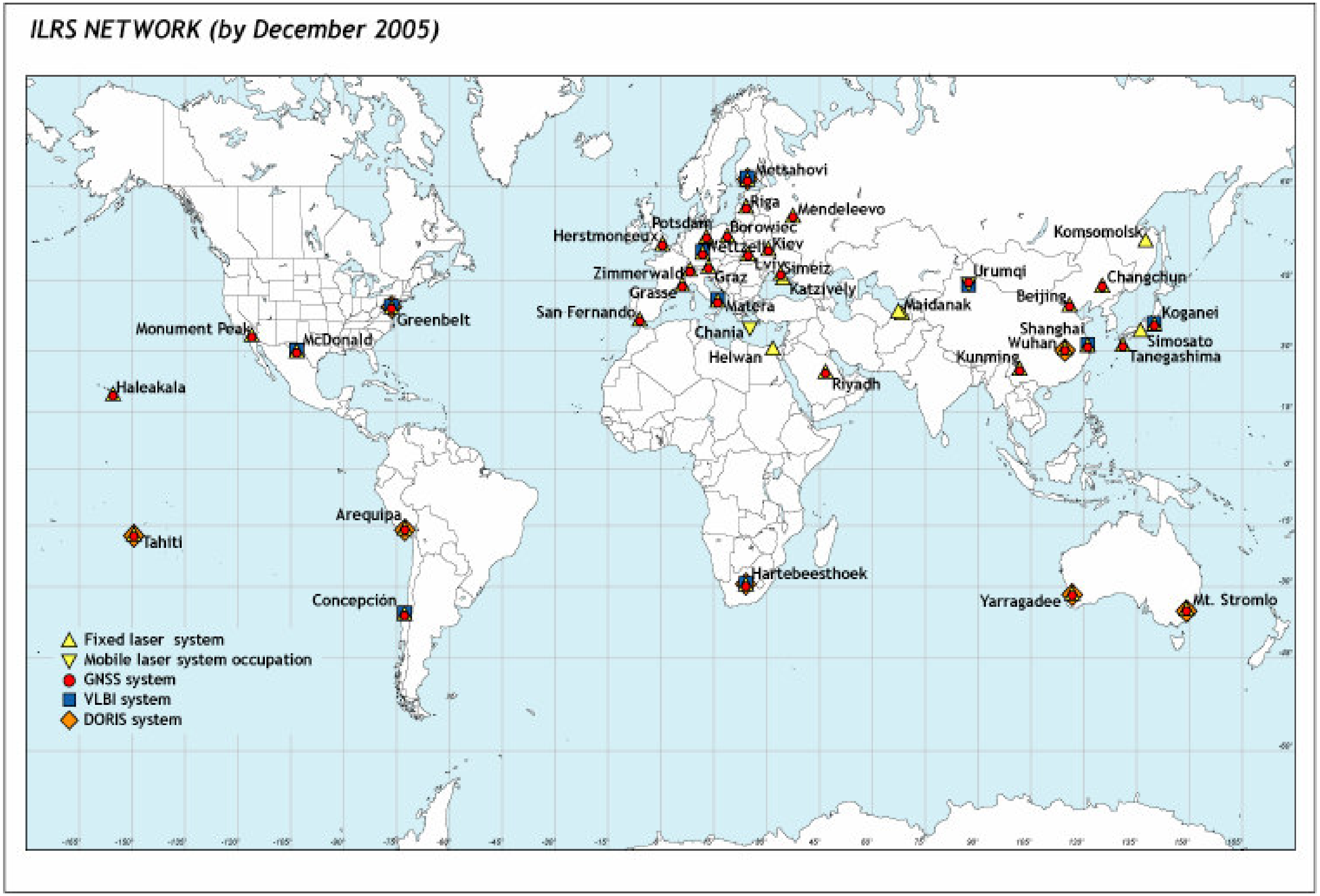

International Laser Ranging Service (ILRS)

- Established in 1998 as a service under the International Association of Geodesy (IAG)
- ILRS collects, merges, analyzes, archives and distributes satellite and lunar laser ranging data to satisfy a variety of scientific, engineering, and operational needs and encourages the application of new technologies to enhance the quality, quantity, and cost effectiveness of its data products
- Components
  - ☞ Tracking Stations and Subnetworks
  - ☞ Operations Centers
  - ☞ Global and Regional Data Centers
  - ☞ Analysis and Associate Analysis Centers
  - ☞ Central Bureau
- ILRS produces standard products for the scientific and applications communities.

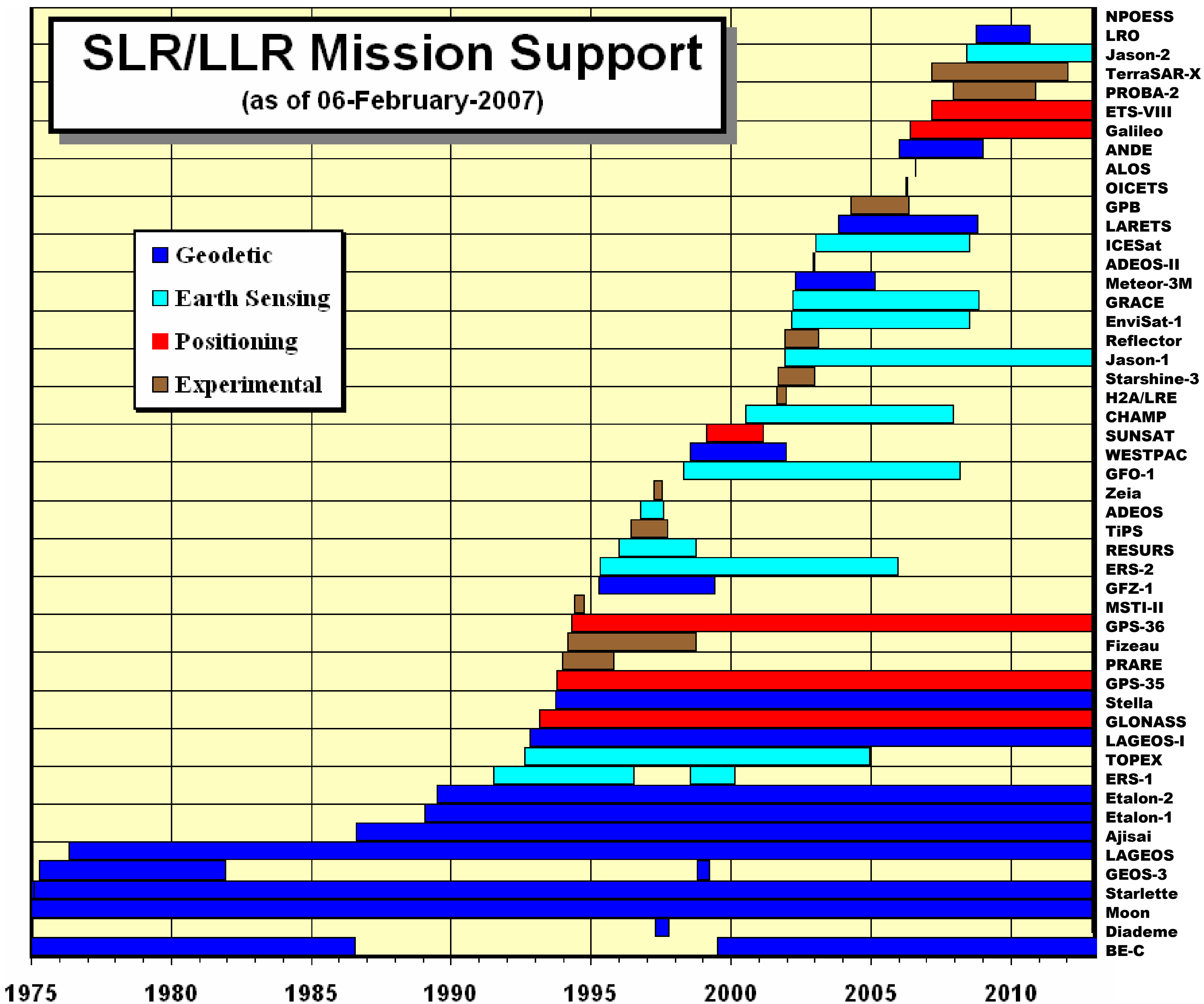
SLR/LLR Mission Support
(as of 06-February-2007)
Geodetic
Earth Sensing
Positioning
Experimental
NPOESS
LRO
Jason-2
TerraSAR-X
PROBA-2
ETS-VIII
Galileo
ANDE
ALOS
OICETS
GPB
LARETS
ICESat
ADEOS-II
Meteor-3M
GRACE
EnviSat-1
Reflector
Jason-1
Starshine-3
H2A/LRE
CHAMP
SUNSAT
WESTPAC
GFO-1
Zeia
ADEOS
TiPS
RESURS
ERS-2
GFZ-1
MSTI-II
GPS-36
Fizeau
PRARE
GPS-35
Stella
GLONASS
LAGEOS-I
TOPEX
ERS-1
Etalon-2
Etalon-1
Ajisai
LAGEOS
GEOS-3
Starlette
Moon
Diademe
BE-C
1975
1980
1985
1990
1995
2000
2005
2010

Distribution of Space Geodesy Co-Location Sites Since 1999

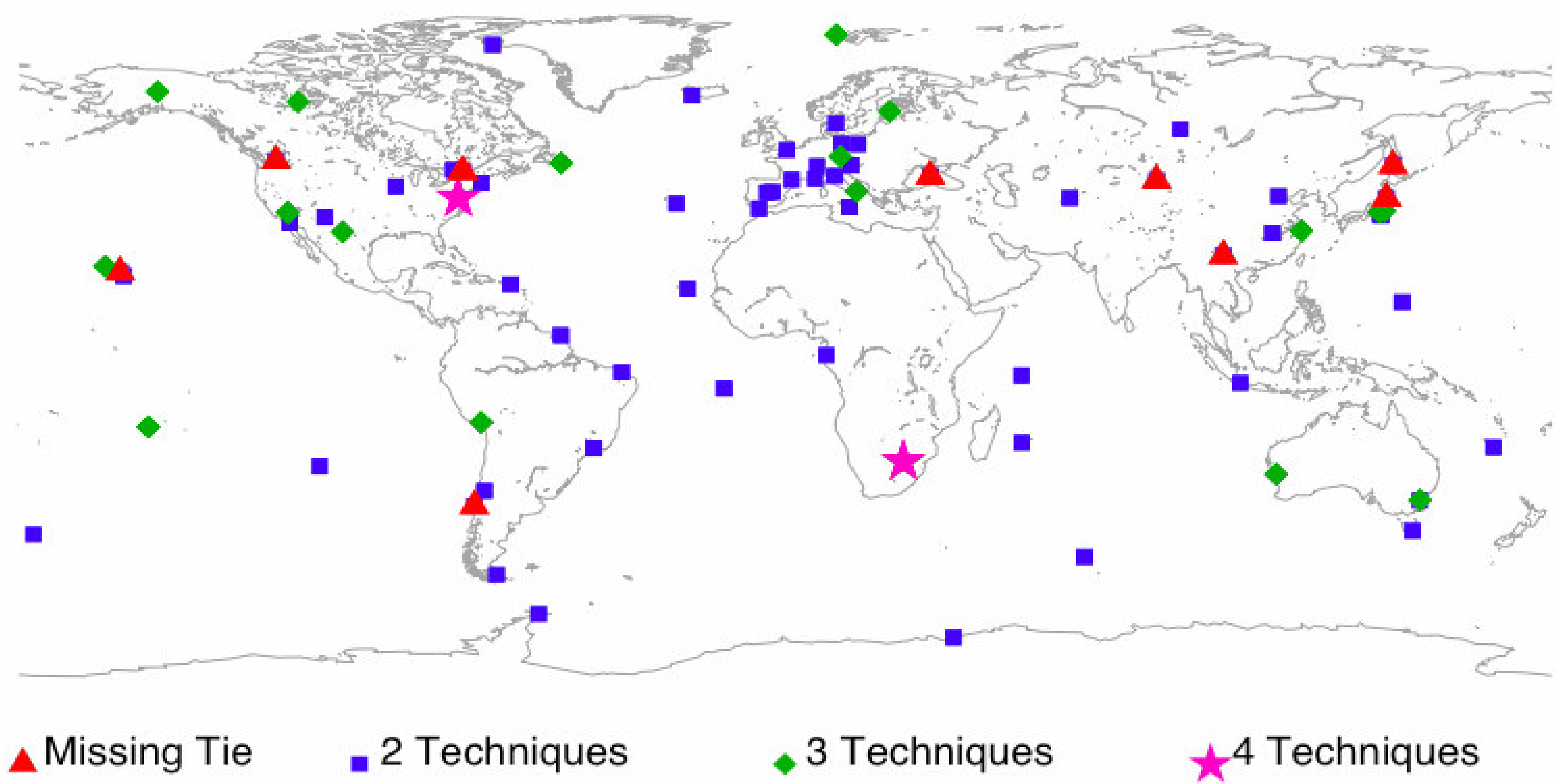

Space Geodesy

GNSS station in Thule, Greenland (photo courtesy of F.B. Madsen, DNSC)

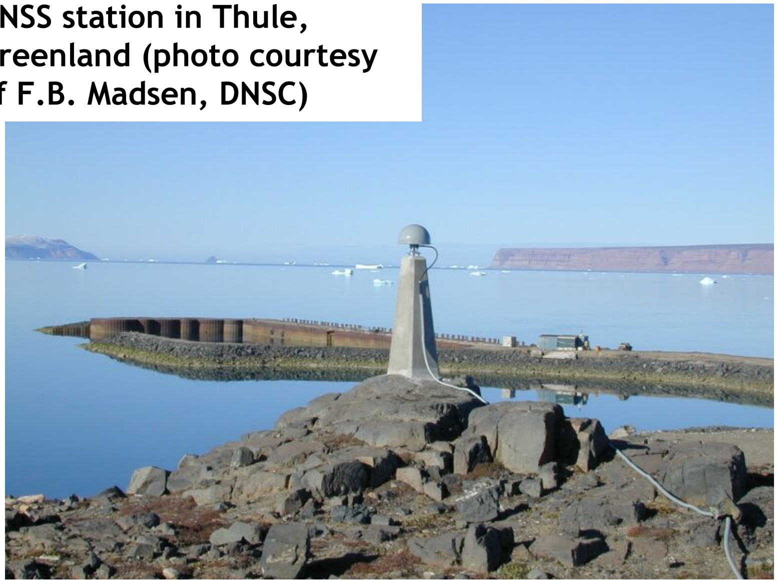

MLRO SLR facility at Matera, Italy (photo courtesy of G. Bianco/ASI)

32-meter VLBI antenna in Tskuba, Japan (photo courtesy of K. Takashima, GSI

DORIS antenna in Tahiti, Fr. Polynesia (photo courtesy of H. Fagard, IGN)

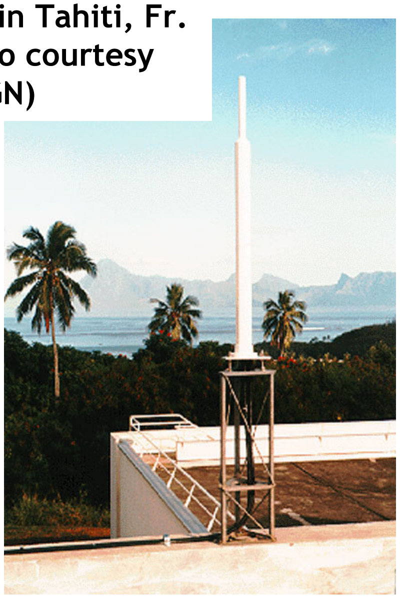

Selected SLR Stations Around the World

Position of Arequipa, Peru

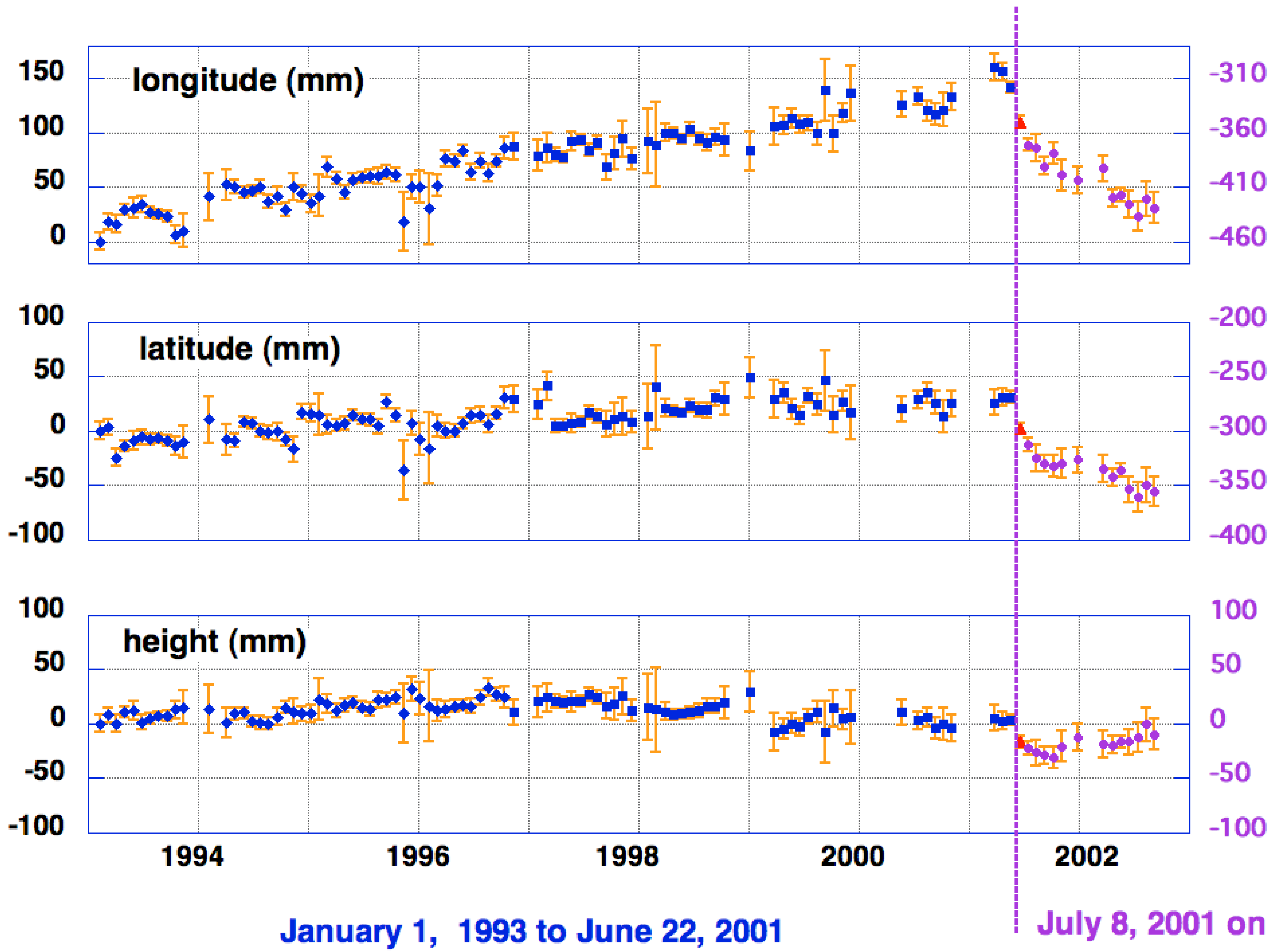

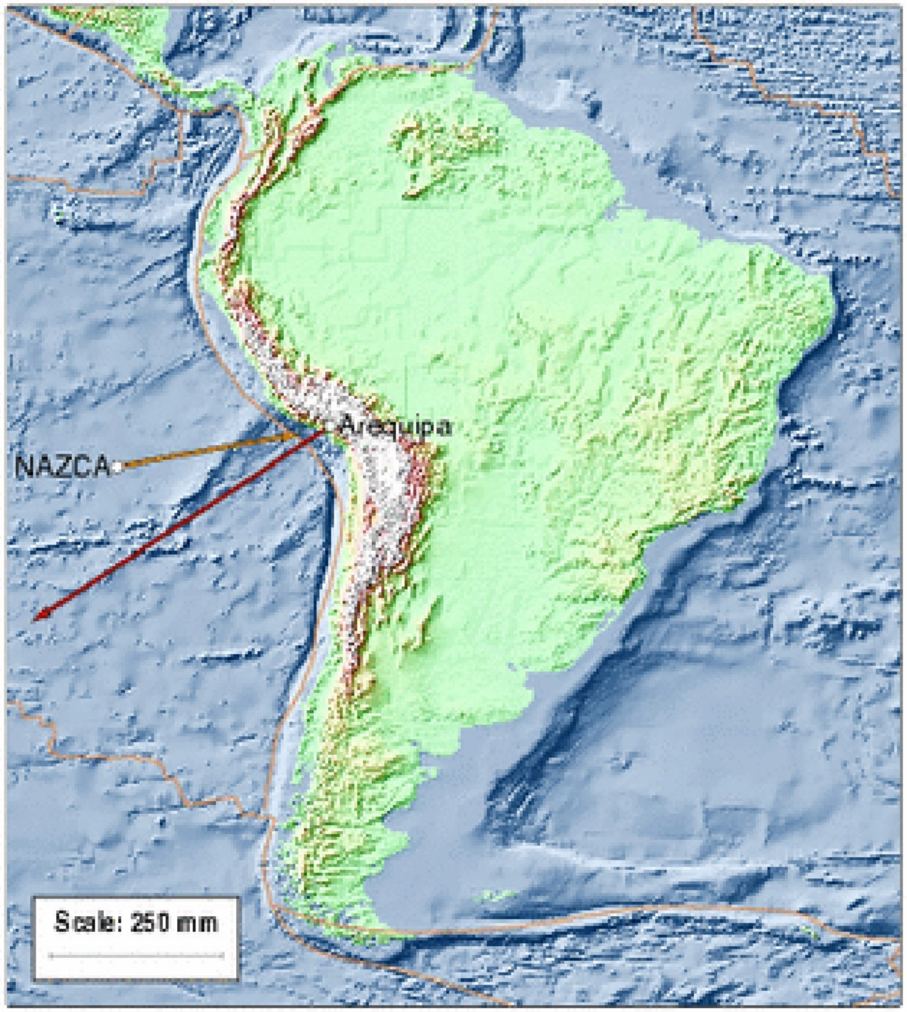

direction of NAZCA motion   53 cm. shift due to M8.4 shock

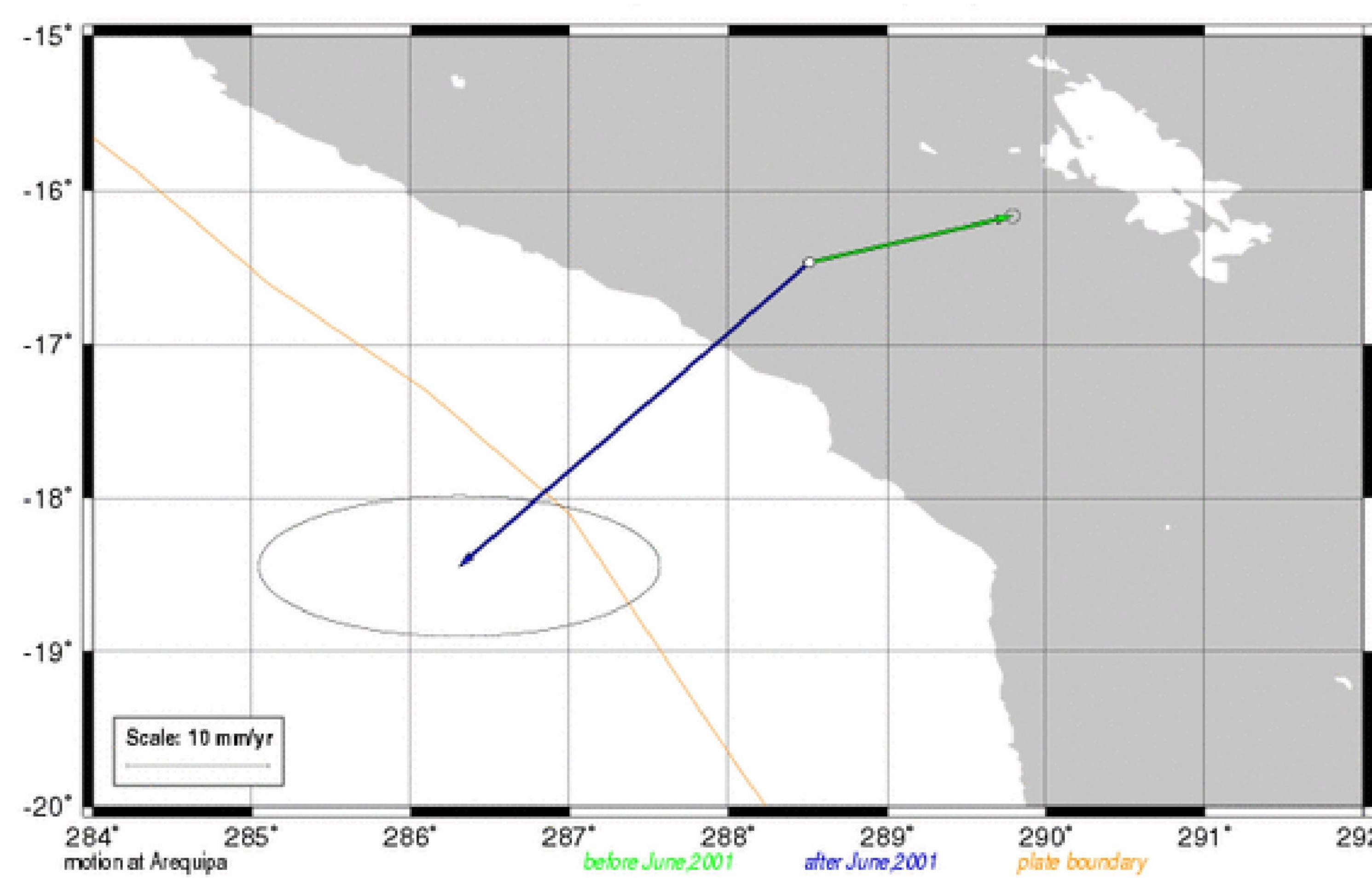

-15°
-16°
-17°
-18°
-19°
-20°
284°
285°
286°
287°
288°
289°
290°
291°
292°
Scale: 10 mm/yr
motion at Arequipa
before June,2001
after June,2001
plate boundary

Arequipa is a vital component of the Reference Frame

International Program for Geodetic Monitoring: "Decade of Geopotential"

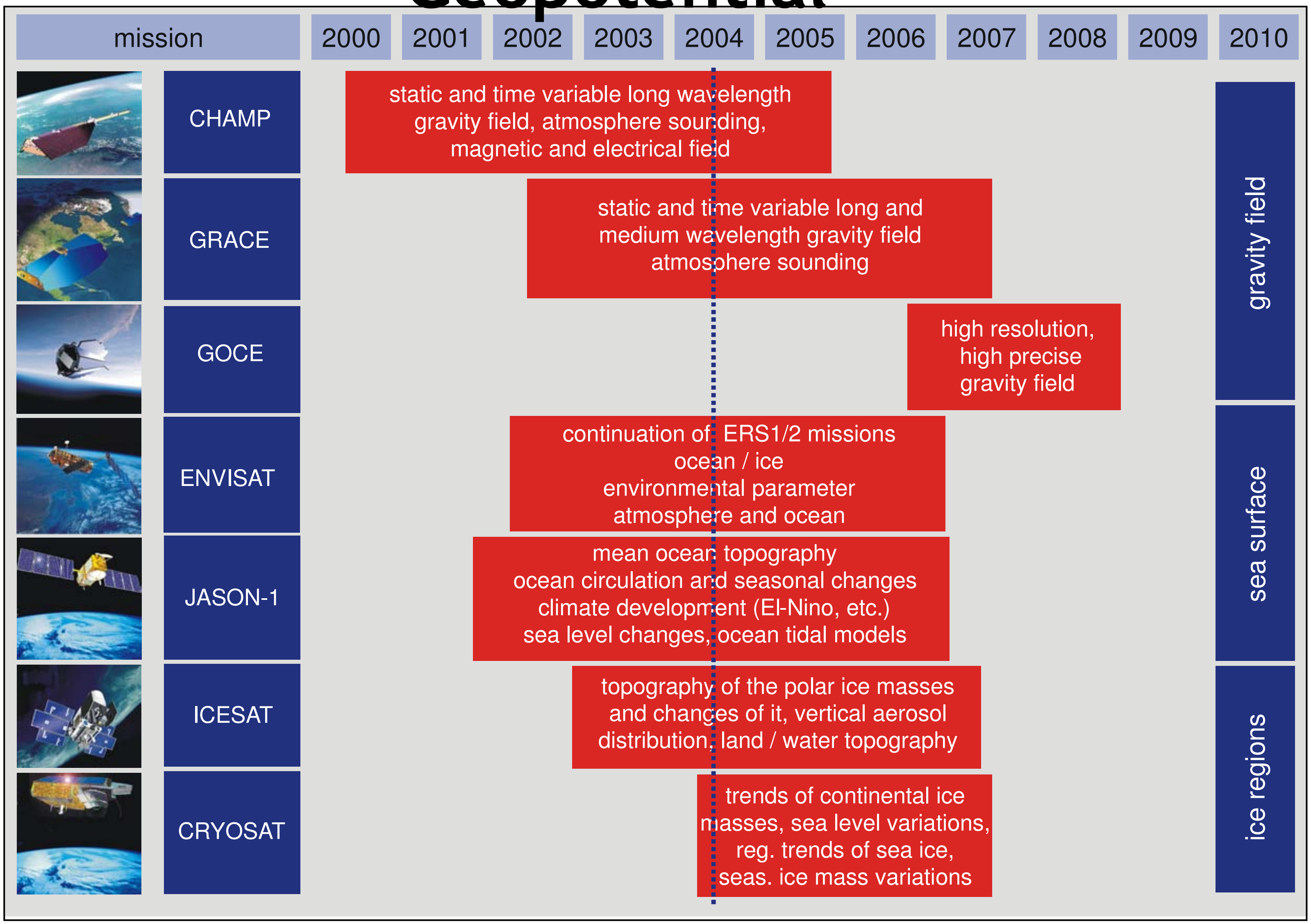

Constituents of an integrated geodetic-geodynamic monitoring system

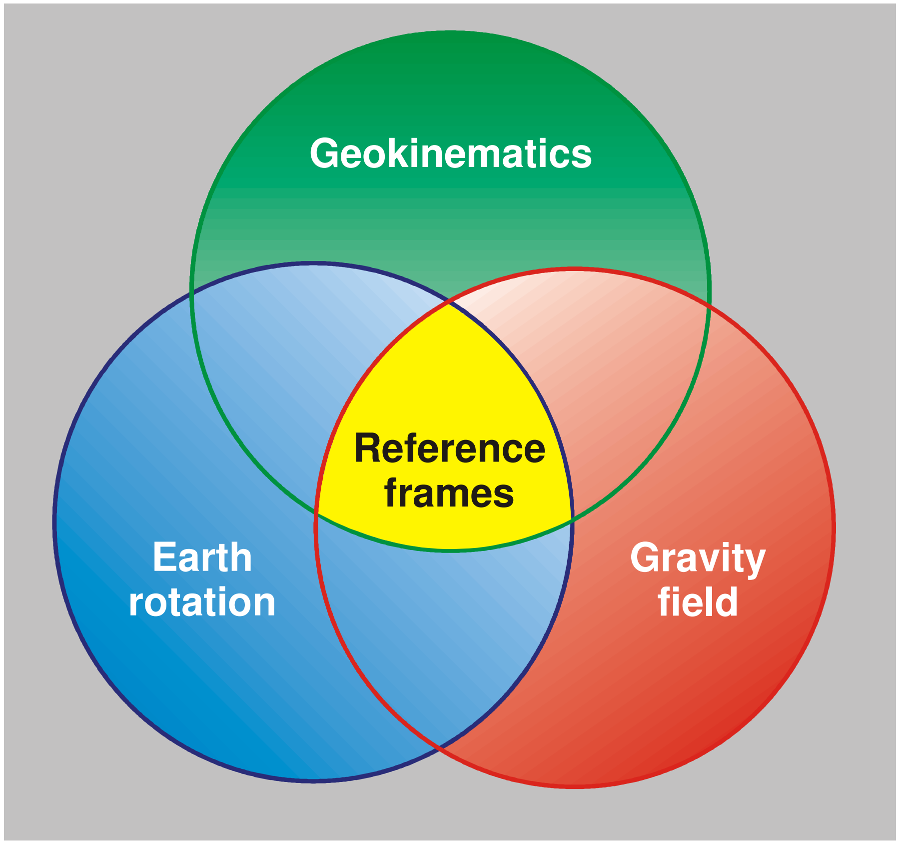

The Vision: Planetary Applications

The State of the Art in Planetary Spacecraft Orbit Determination

- The most precise planetary orbit determination is for Mars Global Surveyor (MGS) operating in orbit at Mars since Sept. 1997.

- The orbital "accuracy" evaluated by laser altimeter cross-overs is ~ 1 meter rms radially and 100 meters horizontally.

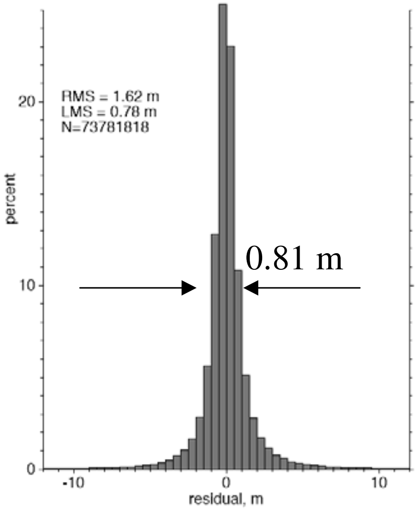

- The tracking of MGS is X-band doppler with precision ~ 50 microns/s every 10 seconds.

- <u>How much better could we do if we tracked planetary orbiters using laser transponders?</u>

The Vision: Lunar Applications

Laser Tracking Scenario for a Lunar Orbiter - 1

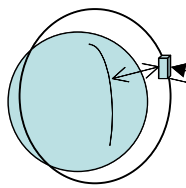

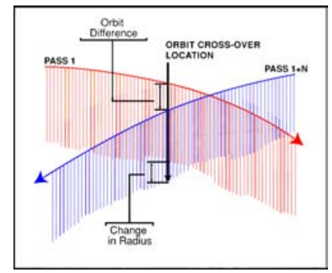

- Consider a lunar geodetic satellite carrying a <u>10 cm laser altimeter</u> and a <u>laser transponder</u> operating in conjunction with an SLR station with SLR2000 performance.

- The laser altimeter operates continuously over both the near-side and far-side of the Moon:
  - it provides the distance of the spacecraft from the surface of the Moon continuously, and
  - it provides cross-over observations that can be used as tracking data.

The Vision: Lunar Applications

Extracting the Far-side Gravity Field of the Moon

- Present knowledge based upon Clementine and Lunar Prospector S-band tracking:
  - ± 20 mGal near-side
  - ± 100 mGal far-side
- Science needs ± 1 mGal

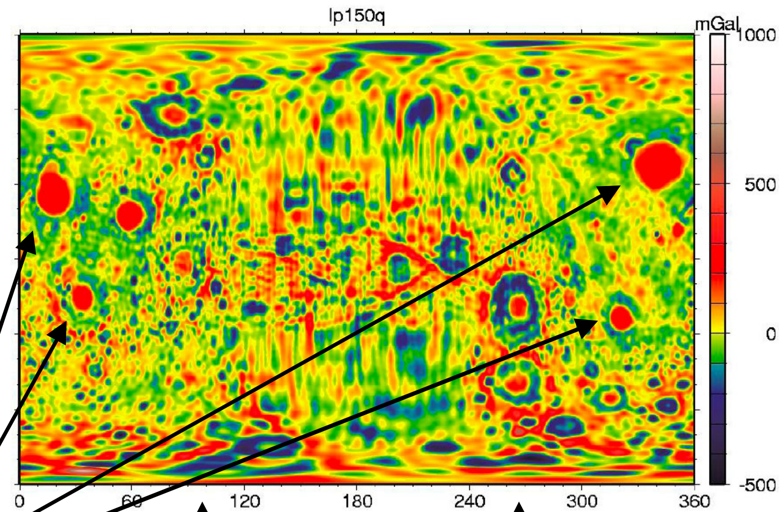

“Mascons”

Lunar Far-side

Striping indicates unresolved gravity signal

---

1 mGal = 10^{-5} meters/sec^2

The Vision: Lunar Applications

Transponder-Laser Ranging Requirements for Science

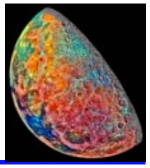

- The tracking requirements of a lunar satellite tracking system are similar to those for geodetic Earth satellites:

  - sub-centimeter ranging;
  - 10 µm/sec velocity (derivable for the range?)
  - 5-second normal points (~ 8km along track)

[*Mircowave tracking at X-band provides 2 meter ranges, ~50 µm/sec velocity at 10-second intervals; Ka-band tracking "can" provide ~40 cm ranges, ~20 µm/sec at 10 second intervals. Weather limitations at Ka-band*]

- Provide the timing system for the spacecraft instrumentation at the 0.1 millisecond level (the transfer of GPS timing to the Moon.